



Investigation of a Transcritical CO₂ Heat Pump in a District Heating Network with Excess Heat from a Power-to-X Facility

Martin Mylin Jensen

Thermal Energy & Process Engineering, TEPE-1011, 2025-06

4th Semester M.Sc.- Master's Thesis





AALBORG UNIVERSITY
STUDENT REPORT

AAU Energy
Aalborg University
<http://www.aau.dk>

Title:

Investigation of a Transcritical CO₂ Heat Pump in a District Heating Network with Excess Heat from a Power-to-X Facility

Theme:

Master's Thesis

Project Period:

Spring Semester 2025

Project Group:

TEPE4-1011

Participants:

Martin Mylin Jensen

Supervisor:

Mads Pagh Nielsen

Number of Pages: 60

Date of Completion:

May 28th - 2025

Abstract:

The thesis investigates the performance and economic feasibility of integrating a transcritical CO₂ heat pump into Aalborgs district heating network, with a focus on utilising excess heat from a future Power-to-X facility. A steady-state model of one 44.25 MW module showed a COP of 3.35, while the dynamic model, which accounts for seasonal variations and transient behaviour, yielded a lower COP of 2.33. The inclusion of a stratified hot water storage tank improved system flexibility and slightly increased efficiency. A shell-and-tube heat exchanger was modelled to preheat seawater entering the evaporator using excess heat. This raised the inlet temperature only between 0.6 and 2.3 K and improved COP marginally from 0.0256 to 0.0431. The economic analysis revealed that the capital cost of the heat exchanger was estimated at €14.7M and was not justified by the operational savings linked to the increased COP. Present worth value calculations over 20 years showed that the system without the heat exchanger was more economically viable. In conclusion, while the transcritical CO₂ heat pump is technically effective and environmentally beneficial, the integration of excess heat via a large-scale heat exchanger is not currently cost-effective. The study recommends further optimisation and exploration of alternative configurations to improve both performance and economic viability.

The content of this report is freely available and may be used in publications with reference. By accepting the request from the fellow student who uploads the study groups project report in Digital Exam System, you confirm that all group members have participated in the project work, and thereby all members are collectively liable for the contents of the report. Furthermore, all group members confirm that the report does not include plagiarism.

Summary

The thesis titled "Investigation of Transcritical CO₂ Heat Pump in a District Heating System with Excess Heat from a Power-to-X Facility" explores the integration of a large-scale transcritical CO₂ heat pump into the district heating network of Aalborg, Denmark. The motivation stems from the global need to decarbonise the heating sector, which is responsible for a significant share of energy consumption and CO₂ emissions. Denmark's ambitious climate goals, including full decarbonization of its district heating network by 2030, provide the backdrop for this study. The project focuses on a 177 MW heat pump system being implemented by Aalborg Forsyning, which will replace the coal-fired Nordjyllandsværket CHP plant and utilise seawater from the Limfjord Strait as its heat source.

The thesis begins with a comprehensive overview of the Danish district heating landscape, highlighting the increasing role of renewable energy and the potential of excess heat from industrial sources and future Power-to-X facilities. It introduces the concept of transcritical CO₂ heat pumps, emphasising their environmental benefits, such as low global warming potential and high efficiency in high-temperature applications. The unique thermodynamic properties of CO₂, including its behaviour in the supercritical region, are discussed in detail, along with the implications for heat exchanger design and system operation.

The core of the thesis is the development of both steady-state and dynamic models of the heat pump system. The steady-state model provides a baseline performance evaluation, yielding a *Coefficient of Performance* (COP) of 3.35 under ideal conditions. The dynamic model, which incorporates time-dependent variables such as seawater temperature and district heating demand, reveals a lower COP of 2.33. This discrepancy underscores the importance of dynamic modelling in capturing real-world performance. The dynamic model also includes a stratified hot water storage tank, which enhances system flexibility by allowing the heat pump to operate more efficiently during periods of low electricity prices and to store energy for peak demand.

A significant part of the thesis is dedicated to evaluating the potential benefits of integrating excess heat from the future Fjord PtX facility. This is achieved through the design and modelling of a shell-and-tube heat exchanger that preheats the seawater entering the evaporator. The heat exchanger is modelled using the ϵ -NTU method and is dimensioned for worst-case scenarios. The analysis shows that the temperature increase achieved is modest, ranging from 0.6 to 2.3 °C, and the corresponding COP improvement is relatively small, between 0.0256 and 0.0431. Despite the technical feasibility, the economic analysis reveals high capital expenses of the shell-and-tube heat exchanger, estimated at €14.7M, outweighing the operational savings. The present worth value analysis over a 20-year period confirms that the system without the heat exchanger is more economically viable.

The thesis also explores alternative configurations and improvements to the heat pump system. These include connecting the heat pumps in series or cascade, implementing mul-

tistage gas cooling, and adding internal heat exchangers to improve vapour superheating. Each of these configurations offers potential efficiency gains and operational flexibility, though they are not modelled in detail within the scope of this work.

In conclusion, the thesis demonstrates that transcritical CO₂ heat pumps are promising for sustainable district heating, particularly when integrated with thermal storage. However, the addition of a large-scale heat exchanger for excess heat integration is not currently economically justified. The study provides a solid foundation for future research, recommending further exploration of alternative heat exchanger designs, parameter sensitivity studies, and improved statistical modelling of seawater temperatures. These efforts could lead to more accurate performance predictions and better investment decisions in the ongoing transition to carbon-neutral heating systems.

Preface

This master's thesis report is written by the TEPE-1011 group, consisting of student Martin Mylin Jensen and supervised by AAU Professor Mads Pagh Nielsen. The project aims to investigate the state-of-the-art transcritical CO₂ heat pump at Aalborg Forsyning. I would like to acknowledge my supervisor for the fantastic sparring and supervision. I would also like to thank the personnel from Aalborg Forsyning for letting me investigate their upcoming heat pump - here goes a special thank you to René Vixø Pedersen and Silas Alvin Hupfeldt. Lastly, thank you to MAN Energy Solutions project manager Mr. Daniel Häny for providing data on the heat pump.

Expectations for the Reader

It is expected that the reader have a general knowledge of thermodynamic principles.


Reading Guide for the Project

Throughout the report, various tables, figures, and equations have been used, which all will be numbered individually. The references implemented throughout the report follow the Harvard referencing method. The models developed and used in this thesis are attached externally.

The following software and hardware are used in the project:

- F-Chart Software - Engineering Equation Solver (EES)
- Mathworks - MATLAB
- Refpropm and CoolProp extensions for Matlab
- Microsoft - Office365
- Overleaf - LaTeX
- Draw.io
- Inkscape

Martin Mylin Jensen

Signature: 

Nomenclature

Symbol	Explanation	Unit
A	Area	m^2
c_p	Specific heat capacity	$\text{J}/(\text{kg}\cdot\text{K})$
C	Heat capacity rate, min, max, c, h	W/K
C	Base cost and cost of equipment	€
C_R	Capacity ratio	—
COP	Coefficient of Performance	—
D	Diameter	m
E	Energy Content	J
f	Friction factor	—
h	Specific enthalpy	kJ/kg
H	Enthalpy	kJ
k	Thermal conductivity	$\text{W}/(\text{m}\cdot\text{K})$
K_L	Minor loss coefficient	—
L	Length	m
\dot{m}	Mass flow rate	kg/s
M	Exponent in cost estimation formula	—
NTU	Number of Transfer Units	—
P	Pressure	Pa
ΔP	Pressure Loss	Pa
Pr	Prandtl number	—
\dot{Q}	Heat transfer rate	W
Q	Capacity measure and base size of equipment	m^2
r	Interest rate	—
Re	Reynolds number	—
T	Temperature	K
\dot{V}	Volume flow rate	m^3/s
U	Overall heat transfer coefficient	$\text{W}/(\text{m}^2\cdot\text{K})$
UA	Overall heat conductance	W/K
V	Volume	m^3
\dot{W}	Pump Work	W/s
ρ	Density	kg/m^3
ϵ	Effectiveness of heat exchanger	—
Φ	Flux limiter function	—
$\hat{\theta}$	Shaping function	—

Abbreviation	Explanation
AE	Algebraic Equation
CAPEX	Capital Expenses
CCS	Carbon Capture and Storage
CC	Carbon Capture
CEPCI	Chemical Engineering Plant Cost Index
CHP	Combined Heat and Power
COP	Coefficient of Performance
CWS	Cold Water Storage
DAE	Differential-Algebraic Equation
DH	District Heating
DHN	District Heating Network
DHW	Domestic Hot Water
EES	Engineering Equation Solver
E-SAF	Electro-Sustainable Aviation Fuel
GWP	Global Warming Potential
HFC	Hydrofluorocarbon
HFO	Hydrofluoroolefin
HP	Heat Pump
HWS	Hot Water Storage
HX	Heat Exchanger
LP	Load Point
MAN	MAN Energy Solutions
MOA	Method of Lines Approach
NJV3	Nordjyllandsværket Block 3
ODP	Ozone Depletion Potential
ODE	Ordinary Differential Equation
OPEX	Operational Expenses
PtX	Power-to-X
PWV	Present Worth Value
Re	Reynolds Number
STHX	Shell-and-Tube Heat Exchanger
TC	Transcritical
VC	Vapour Compression

Contents

1	Introduction	1
1.1	District Heating in Denmark	2
1.1.1	Excess Heat in the District Heating Network	3
1.2	District Heating in Aalborg	3
1.3	Heat Pump Cycle	6
1.3.1	Transcritical CO ₂ Heat Pump Cycle	6
1.4	CO ₂ as a Natural Refrigerant	8
2	Problem Statement	13
2.1	Methodology	13
3	Modeling	14
3.1	System Breakdown and Topology	14
3.2	Steady-State Transcritical Heat Pump Model	15
3.3	Heat Exchanger Model for Excess Heat from Fjord PtX	18
3.3.1	Heat Exchanger Dimensions	22
3.3.2	Pressure Losses in the Heat Exchanger	23
3.4	Dynamic Model of District Heating System	24
3.4.1	Discretisation of Gas Cooler and Evaporator	26
3.4.2	Conservation of Energy and Mass	27
3.4.3	Solver and Indexing in Matlab	28
3.5	Thermal Energy Storage	30
4	Results of Dynamic Transcritical Heat Pump Model and Heat Exchanger Model	33
4.1	Dynamic Transcritical Heat Pump Model	33
4.2	Results from Heat Exchanger Analysis	36
4.3	Dynamic Transcritical Heat Pump Model with Hot Water Storage	39
4.3.1	Results from Transcritical Heat Pump Model with Hot Water Storage with Load Point 2 as Reference	42
4.4	Effects of Temperature Rise to the Evaporator by Heat Exchanging with Excess Heat	44
4.5	Improvements and Comments on the Heat Pump Configuration and System at Aalborg Forsyning	47
4.5.1	Heat Pumps in Series	48
4.5.2	Heat Pumps in Cascade	48
4.5.3	Multistage Gas Cooling	49
4.5.4	Internal Heat Exchanger	50
5	Techno-Economic Feasibility Analysis of Heat Exchanger Scenario	51
5.1	Cost Analysis	51
5.1.1	Capital Expenses	51

5.1.2	Operational Expenses	52
5.1.3	Present Worth Value	53
5.1.4	Results of Present Worth Value	53
6	Conclusion	57
7	Future Work	59
7.1	Heat Exchanger Variations	59
7.2	Parameter Study for Dynamic Heat Pump Model	59
7.3	Different Heat Pump Configurations and Adjustments	59
7.4	Statistical Analysis of Seawater Temperatures	60
	Bibliography	61
A		64
A.1	Additional Equations for Hot Water Storage	64

List of Figures

1.1	The evolution of fuels in the district heating network in Denmark from 1975-2020.	2
1.2	Average, maximum and minimum seawater temperatures in the Limfjord Strait measured at Aalborg averaged from 2010-2023. Data provided by Aalborg Forsyning was measured at their location.	4
1.3	Sketch of a Log-Ph diagram of a TC cycle with CO ₂ as the refrigerant. The graph is from the Danfoss CoolSelector2 software.	7
1.4	Sketch of temperature profiles and glides of the heat rejection process in a subcritical compression cycle with ammonia as the refrigerant.	9
1.5	Sketch of temperature profiles and glides of the heat rejection process in a transcritical cycle with CO ₂ as the refrigerant. CO ₂ is at a pressure of 120 Bar.	10
1.6	Transport and thermodynamic properties of CO ₂ across a wide range of pressures and temperatures, covering sub-critical, near-critical, and super-critical regions.	11
1.7	Specific heat capacity of CO ₂	11
3.1	Topology of the system. Inspired by the future DHN in Aalborg and by Aalborg Forsyning.	14
3.2	Sketch of Steady State Heat Pump Model	16
3.3	P-h diagram for the steady-state transcritical heat pump cycle.	17
3.4	COP as a function of time.	18
3.5	The figures above show the excess heat delivery from Fjord PtX to Aalborg Forsyning for each hour, and for the first half of February the same year [Aalborg Forsyning, 2025]	19
3.6	Illustration of the STHX used for the excess heat scenario.	20
3.7	The figures above show the heating demand for Aalborg Forsyning for each hour, throughout 2024, and for two selected days during February the same year ie. in the LP1 period. The data is from 2024. [Aalborg Forsyning, 2025]	25
3.8	Supply and return temperature of the district heating water to and from Aalborg Forsyning. [Aalborg Forsyning, 2025]	26
3.9	Spatial discretisation of the gas cooler. Discretisation inspired by [Holten et al., 2012] and [Nielsen and Sørensen, 2020].	27
3.10	Indexing used in the Matlab model. Indexing inspired by [Holten et al., 2012] and [Nielsen and Sørensen, 2020].	29
3.11	Stratified water storage tank with notation and discretisation. Inspired by [Kreuzinger et al., 2008].	30
3.12	Finite volume discretization of the storage tank where ● denotes cell centres and ○ denotes cell faces. [Kreuzinger et al., 2008]	31
4.1	Ph-Diagram of the dynamic heat pump cycle	34

4.2	Temperature distribution curves in the gas cooler as a function of the dimensionless length of the gas cooler.	34
4.3	Temperature distribution curves in the evaporator as a function of the dimensionless length of the evaporator.	35
4.4	Dynamic start-up response of the district heating water temperature as a function of time.	36
4.5	Temperature increase of the seawater to the inlet of the evaporator when heat is exchanged in the STHX.	37
4.6	Temperature distribution curves in a counterflow STHX as the capacity ratio approaches zero because $\dot{C}_c \gg \dot{C}_h$	38
4.7	Increased pump power to overcome pressure losses in the STHX.	39
4.8	The energy content of the How Water Storage tank as a function of time, in the LP1 period of 48 hours.	40
4.9	Temperature of five selected layers in the HWS as a function of the 48-hour period of LP1.	41
4.10	P-h Diagram of the TC-HP with HWS included	42
4.11	District heating demand in LP2	43
4.12	The energy content in the HWS in LP2	43
4.13	COP of the transcritical heat pump as a function of varying the inlet temperature to the evaporator.	45
4.14	Mass flow rate of CO ₂ variation as a function of the evaporator inlet temperature. As the evaporator inlet temperature increases, the mass flow rate of CO ₂ decreases as the distance between isentropes becomes larger.	46
4.15	COP as a function of the evaporator inlet temperature. The shaded areas are the COP gain from LP1 and LP2 when evaluated with and without heat exchanging with the excess heat from Fjord PtX.	47
4.16	Two heat pumps in series connection	48
4.17	Two heat pumps connected in a cascade configuration. A high temperature side and low temperature side is present connected with a cascade heat exchanger.	49
4.18	Heat pump cycle with an internal heat exchanger. This ensures only vapour enters the compressor.	50
5.1	Present Worth Value with revenue pick-up. The electricity price is €75/MWh and the interest rate is 8%	55
5.2	Present Worth Value without revenue pick-up. The electricity price is €75/MWh and the interest rate is 8%	56

List of Tables

- 1.1 Overview of the excess heat suppliers and their contribution in the District Heating Network in Aalborg in 2024 [Aalborg Forsyning, 2024]. 5
- 1.2 Properties of some refrigerants. [Zhang and Yamaguchi, 2021] 8

- 3.1 Dimensions of the STHX analysis 22
- 3.2 Heat pump plant annual operating hours, load points and supply and return temperatures. [Aalborg Forsyning, 2025] 24

- 4.1 Temperature differences used to calculate the mass flow of the seawater into the heat exchanger. 37

- 5.1 Results of the economic data. 54

Chapter 1

Introduction

Half of the world's consumption of primary energy sources comes from the heating and cooling sector, with CO₂ emissions accounting for 40% of the total world emissions [MAN, 2023]. The heating sector accounts for 98% of that demand. The energy demand has risen in recent years and is therefore not sustainable for the climate. The demand for renewable and more efficient heating and cooling systems and technologies is critical to prevent climate change and reach the goal of not exceeding a global temperature increase of 2°C as agreed on in the Paris Agreement [United Nations Climate Change, 2022].

Heating and cooling technologies worldwide are still dominated by fossil fuels and a transition to renewable green fuels or a switch to electrical-powered units is in the making. Electrical-powered units like heat pumps are green if the electricity comes from renewable sources like solar, wind or hydropower.

Heat pumps can be used on a small scale for households for space heating and *Domestic Hot Water* (DHW) production. The transition to heat pumps has grown rapidly in recent years, thanks to the financial aid that many governments provide for switching out gas, oil, or even wood pellet furnaces.

Large-scale heat pumps are entering the heating sector as a way of decarbonization. The technology is well-known, robust and efficient. A large-scale heat pump can integrate well into a *District Heating Network* (DHN) where hot water is produced for space heating and DHW for customers. It works great with so-called sector coupling, where other technologies like hot water storage tanks, electric boilers, solar collectors and excess heat are present. This ensures a flexible system that works both at daily and seasonal fluctuations in supply and demand.

State-of-the-art large-scale heat pumps include *Transcritical* (TC) water-to-water heat pumps with CO₂ as a refrigerant. TC CO₂ heat pumps are not a new technology and have been around for 40-50 years, but it has matured to a stage where large-scale units are being built and used for district heating and other industrial purposes. In Esbjerg, Denmark, two 30 MW TC CO₂ water-to-water heat pumps have been built by MAN Energy Solutions. They extract heat from the Wadden Sea. Similarly, in Aalborg, four heat pump units of 44.25 MW each are currently being built with a goal of implementation by the end of 2028. Because of the high pressures, the heat pumps have to withstand due to CO₂'s properties, the compressor, particularly, has to be stronger than traditional sub-critical *Vapour Compression* (VC) heat pumps.

Furthermore, the heat pumps in Esbjerg and Aalborg both draw their energy from the sea. Therefore, the evaporator, which is in direct contact with saltwater, has to be able to withstand increased corrosion. Therefore, these evaporators are typically built in titanium, which makes a big impact on the overall price of the system.

1.1 District Heating in Denmark

Denmark is one of the leading countries in the world when it comes to *District Heating* (DH). The network is wide and constantly expanding. As of 2025, more than 2/3 of Danish households are connected to the DHN. 76.9 % of the district heating comes from renewable energy sources with the goal of full decarbonization in 2030 in place [Dansk Fjernvarme, 2023]. Renewable energy in the DHN can also be as excess heat from the industry, waste incineration plants, *Carbon Capture* (CC) or *Power-to-X* (PtX) facilities.

Previously, the DHN's main energy providers have been *Combined Heat and Power* (CHP) plants, where mainly fossil fuels have been used. Later, renewable fuels like biogas and biomass like wood pellets and straw. Recently, many of the Danish CHP plants are transitioning to large-scale heat pumps. This corresponds well to the trend of a general electrification [Dansk Fjernvarme, 2023]. An overview of the different types of fuels used in the Danish DHN is seen in Figure 1.1.

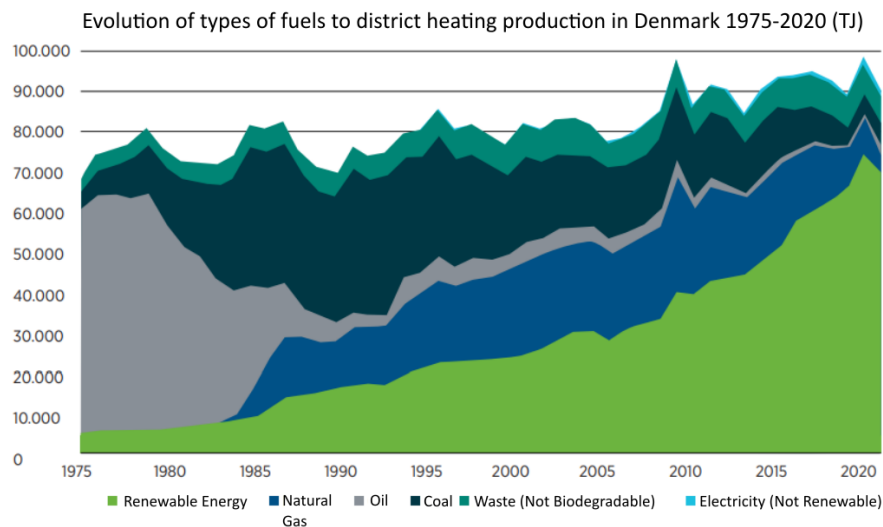


Figure 1.1: The evolution of fuels in the district heating network in Denmark from 1975-2020.

It is evident that renewable energy presently covers most of the fuel consumption in district heating. 48% of the total fuel consumption is based on renewable biomass and is the primary contributor to the district heating, consisting of 76.9% renewable energy [Dansk Fjernvarme, 2023]. The Danish DHN will transition to mainly electric-based heat-

ing methods, like heat pumps and electric boilers. This opens up the possibility of biomass being used for the production of green fuels instead.

1.1.1 Excess Heat in the District Heating Network

One of the DHN's main forces is to collect and reuse excess heat. Many processes generate heat as a by-product, and instead of sending this heat into the atmosphere as a loss, it can be 'harvested' and sent into the DHN. This is clever since the need for new heat production is thereby reduced. The heat can be transferred with a heat exchanger or a heat pump if the excess heat is at a lower temperature than what is required in the DHN. Normally, there is a distinction between high and low-temperature excess heat at approximately 60-65°C. High temperature excess heat can typically be used directly in the DHN, whereas the low temperature excess heat has to be boosted by a boiler or heat pump.

Only around 3.6 % of the DH in Denmark is covered by excess heat, which corresponds to 1400 GWh/year. However, there is a huge amount of excess heat which is not utilised. This is linked to a law and a price cap that monitors how much excess heat the DH companies can use. The law was in place to ensure fair prices for the consumers. As of January 17th 2025, this price cap was revoked, and this opens the door for more excess heat in the DHN [KEFM, 2025]. With the unused excess heat from industry and data centres as well as future CC- and PtX-facilities it is estimated that in 2045 the amount of excess heat in the DHN could be 33 %. This number is highly dependent on many factors, including the distance between the industry and the DHN [Dansk Fjernvarme, 2023].

1.2 District Heating in Aalborg

This master's thesis will revolve around the DHN in Aalborg, Denmark, which Aalborg Forsyning A/S manages. The DHN in Aalborg consists mainly of Nordjyllandsværket (NJV), which is a coal-fired CHP plant with a capacity of 422 MW_{th}. Even though it is one of the most efficient coal-fired CHP plants in the world, the government's climate goals for 2030 concerning reductions of carbon emissions have led to a decision to phase out the CHP plant for the benefit of other systems/technologies. The NJV is situated 13 km outside Aalborg, on the Limfjord Strait's north side.

At the end of 2028, NJV 'Block 3' (NJV3) will be phased out and make way for a new heat pump. This heat pump will be a water source heat pump with CO₂ as the refrigerant flowing in a TC cycle with a total capacity of 177 MW_{th}. MAN Energy Solutions manufactures it and will be the world's largest heat pump of its kind [MAN, 2025]. The heat pump draws its energy from the Limfjord Strait, which has a temperature of -1 - 5°C in the winter and 12-20°C in the summer. Figure 1.2 illustrates the average, maximum and minimum seawater temperature in the Limfjord Strait in the period 2010-2023.

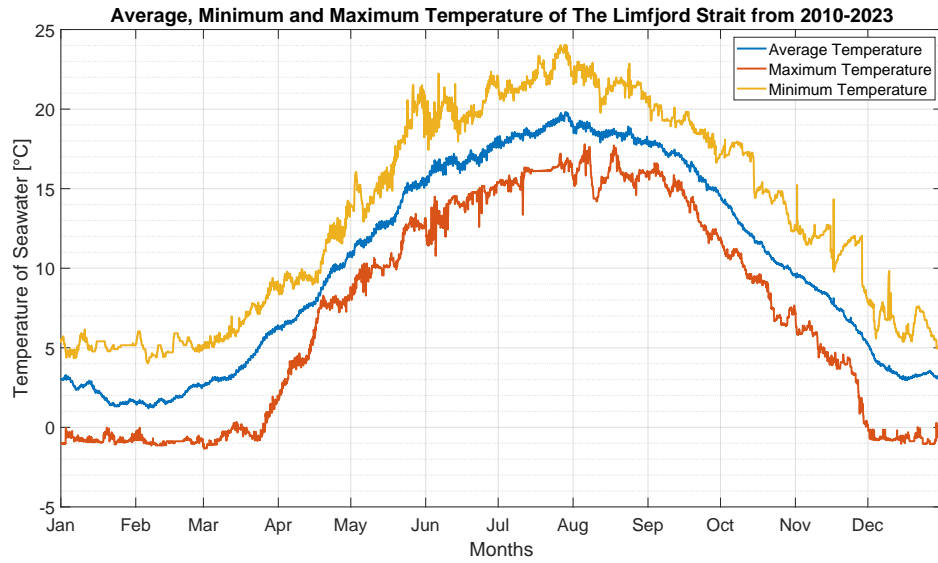


Figure 1.2: Average, maximum and minimum seawater temperatures in the Limfjord Strait measured at Aalborg averaged from 2010-2023. Data provided by Aalborg Forsyning was measured at their location.

Some years, the winter in Denmark is so cold that the water in the Limfjord Strait freezes. The freezing point of seawater depends on the salinity of the water. In the Limfjord Strait, the salinity is around 25‰, which makes the water freeze at approximately -1.5°C . This has happened with varying periods 10 out of the last 14 winters, with the worst in the winters of 2010 and 2011, where the Limfjord Strait was frozen for 130 days in total. With a pinch temperature of 2 K, the heat pump operation is impossible, and it must shut down. This could have huge implications for Aalborg Forsyning and its customers and lead to a strong dependency on auxiliary systems like electric boilers and hot water storage. A tendency of milder winters in Denmark due to climate change could see this phenomenon having less influence in the future.

The heat pump is set to deliver 700.000 MWh/year, which will correspond to around 36.5 % of the demand in Aalborg [Aalborg Forsyning, 2024] and will reduce 160.000 tons of CO_2 emissions yearly compared to the coal-fired CHP plant. Alongside the heat pump, other systems are being constructed as well to give flexibility to the overall system. This will include 4 equally-sized water storage tanks with a total volume of 200.000 m^3 and 3 equally-sized electrical boilers with a total capacity of 150 MW to help with peak loads and boost the water if necessary. This will help with sector coupling in the future.

Aalborg Forsyning also retrieves excess heat from industries in the area. This is mainly from two sites - the cement factory 'Aalborg Portland' and the waste incineration plant 'Nordværk' - which as of 2024 delivered a combined 92.4 % of the total excess heat in the DHN in Aalborg. In Table 1.1, all of the excess heat suppliers are listed alongside their contributions.

Table 1.1: Overview of the excess heat suppliers and their contribution in the District Heating Network in Aalborg in 2024 [Aalborg Forsyning, 2024].

Excess Heat Supplier	Heat [GJ]	Heat [MWh]
Nordværk I/S	1.312.485	364.579
Aalborg Portland A/S	1.057.414	293.726
Electric Boiler - Norbis Park	157.994	43.873
Water Treatment Plant Øst	7200	2000
IKEA Aalborg	8618	2393
Ulsted Biogas Aps	2504	696
Aalborg Crematorium	5098	1416
Water Treatment Plant Vest	3971	1103
Others	1103	306
Kyoto - Norbis Park	3483	968
Excess Heat Total Share	2.564.085	712.245
Total District Heat Delivered	6.896.991	1.915.831

The amount of excess heat supplied from 'Nordværk' and 'Aalborg Portland' is enough to cover the district heating demand in the summer half-year. In 2024, the amount of excess heat used for district heating in Aalborg was 37.2 %, however, as mentioned earlier, this could become higher now that the price cap has been revoked.

As of March 12th 2025, during the writing of this thesis, Aalborg Portland finalised their *Carbon Capture and Storage* (CCS) facility agreement [Aalborg Portland, 2025]. This CCS facility will provide excess heat corresponding to 19.000 households per year or between 260.000-344.000 MWh/year, depending on which average heat consumption for a household is used [Dansk Fjernvarme, 2024]. This amount of excess heat corresponds to the current amount that is delivered from Aalborg Portland.

Plans for a 585 MW PtX facility, Fjord PtX, are currently being prepared. The facility is set to be in operation in 2030. This PtX-facility will synthesise 75,000 tons *Electro Sustainable Aviation Fuel* (E-SAF) yearly. This will be done using carbon dioxide captured from Nordværk's CC-process. Fjord PtX will have excess heat available from the hydrolysis and synthesis processes for Aalborg Forsyning to use for district heating. Fjord PtX is set to provide excess heat corresponding to 11.000 households per year or between 150.000-200.000 MWh/year, depending on which average heat consumption for a household is used [Fjord PTX, 2025] [Dansk Fjernvarme, 2024]. Fjord PtX will provide

both high- and low-temperature excess heat. Still, it is estimated that Aalborg Forsyning will only be able to accept the high-temperature excess heat from the methanol-synthesis [Aalborg Forsyning, 2025]. Therefore, the low-temperature excess heat from the hydrolysis will have to be cooled locally, which requires energy. It is estimated that the low-temperature excess heat from Fjord PtX will have a capacity of between 29.8 and 51.6 MW at a temperature of 67°C [Aalborg Forsyning, 2025]. The water is wastewater from the hydrolysis process. It is therefore inappropriate to mix with either the inlet to the heat pump or the district heating supply, and the heat must be transferred in a heat exchanger.

1.3 Heat Pump Cycle

A heat pump utilises electricity to move heat from a colder side to a hotter side. There are many different types of heat pumps, but they mainly differ in two ways. The cold-temperature reservoir, for instance, air, ground, or water and which refrigerant used as the heat-transferring medium. A heat pump has four main components: Evaporator, compressor, condenser and expansion valve. The heat pump operates within a closed loop where a refrigerant flows and operates as a heat-transferring medium, where the latent heat of vaporisation is used.

The efficiency of a heat pump is denoted as the *Coefficient of Performance* (COP), which is described as the desired output compared to the work inserted in the compressor as seen in Equation 1.1.

$$\text{COP}_{\text{HP}} = \frac{Q_H}{W_c} \quad (1.1)$$

Where Q_H is the thermal capacity out of the gas cooler and W_c is the power drawn to the compressor. Several factors influence the COP, such as the temperature of the heat source and sink and the type of refrigerant.

If renewable energy sources power the compressor and the evaporator draws its energy from a renewable source, like ambient air or, in the case of this thesis, the Limfjord Strait, the system is essentially a carbon-neutral heat-delivering system.

1.3.1 Transcritical CO₂ Heat Pump Cycle

The basics of a TC heat pump cycle with CO₂ are the same as a normal VC cycle, but with some deviations. Transcritical means that the refrigerant, ie. CO₂ is compressed from saturated vapour to superheated vapour in the supercritical state. This means above its critical point, see Figure 1.3 of a basic log-Ph diagram of a TC cycle with CO₂. The figure is not of any particular case, but serves as a sketch of a general TC cycle.

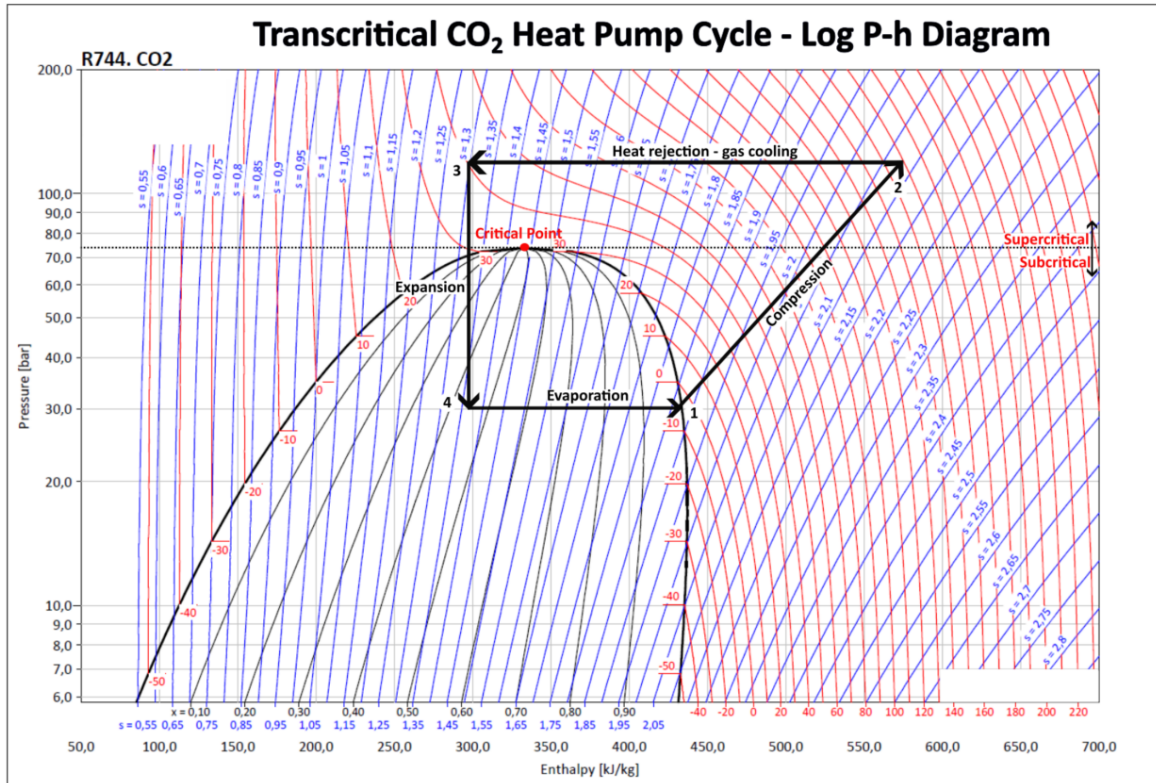


Figure 1.3: Sketch of a Log-Ph diagram of a TC cycle with CO₂ as the refrigerant. The graph is from the Danfoss CoolSelector2 software.

From 4-1, the refrigerant is in contact with the cold-source reservoir/external heat sink ie. the Limfjord Strait in this case, where the refrigerant is evaporated in an isothermal evaporation process to a saturated vapour. From 1-2, the refrigerant is compressed isentropically by a compressor from saturated vapour to superheated gas in the supercritical region. Here, the pressure and temperature are increased. From 2-3, the compressed gaseous refrigerant enters the gas cooler, where it transfers heat isobarically to the hot-temperature reservoir ie. the district heating supply. Heat is rejected as the gas is cooled without phase change if the temperature is not lowered beyond the critical temperature. The heat rejection process is one of the most particular processes in TC cycles because heat is rejected by single-phase cooling instead of condensation as in conventional sub-critical cycles. This is why it is called a gas cooler instead of a condenser. It also happens at constant pressure rather than constant temperature. Gas cooling processes with CO₂ also have a higher temperature, which fits the water heating process better [Zhang and Yamaguchi, 2021]. Lastly, from 3-4, the refrigerant is expanded by an expansion/throttling valve isenthalpic from high pressure to low pressure and the cycle repeats. In this step, the refrigerant changes phase, whereas a normal sub-critical heat pump has the phase change from gas to liquid in the condenser.

The COP of a heat pump can be calculated with Equation (1.1) but also by the change in specific enthalpies from different points in the cycle seen in Equation (1.2).

$$\text{COP}_{\text{HP}} = \frac{Q_H}{W_c} = \frac{h_2 - h_3}{h_2 - h_1} \quad (1.2)$$

Where h_1 is the enthalpy before compression, h_2 is the enthalpy after the compression before it enters the gas cooler, h_3 is the enthalpy after the gas cooler, which is equal to h_4 since the expansion is considered isenthalpic.

1.4 CO₂ as a Natural Refrigerant

CO₂ or R744 is proposed as a very promising refrigerant but with different thermodynamic properties than standard refrigerants. R744 is a natural refrigerant and is known for its environmental friendliness. It has an *Ozone Depletion Potential* (ODP) of 0 and a *Global Warming Potential* (GWP) of 1. GWP is a measure of the potency of a refrigerant compared to CO₂e. The GWP of CO₂ is significantly lower than traditional HFCs, CFCs, HCFCs and the new synthetic HFOs, which are in the range of 100-10,000. CO₂ is also non-toxic and non-flammable [Zhang and Yamaguchi, 2021]. Some refrigerant properties are seen in Table 1.2.

Table 1.2: Properties of some refrigerants. [Zhang and Yamaguchi, 2021]

Properties	R717 (Ammonia)	R744 (CO ₂)	R290 (Propane)	R22 (HCFC)	R134a	R1234ze(E)
ODP/GWP	0/0	0/1	0/6	0.05/1700	0/1300	0/0
Flammability/Toxicity	B2L	A1	A3	A1	A1	A2L
Critical Pressure (MPa)	11.42	7.38	4.25	4.97	4.07	3.6
Critical Temperature (°C)	133	31.1	96.7	96	101.1	109.4

In the EU, a trend towards using natural refrigerants instead of traditional and synthetic refrigerants is present because they have high GWP or contain fluorine [MAN, 2023]. There is, however, no 'perfect' refrigerant; it comes down to what operation is required and its corresponding requirements for the refrigerant. Different refrigerants have different operation ranges.

CO₂ as a refrigerant also proposes thermodynamic and transport properties. It has a relatively low critical temperature of 31.1°C and a high critical pressure of 7.38 MPa or 73.8 Bar, which is one to two times higher than traditional refrigerants, see Table 1.2. These properties allow for CO₂ to work in the supercritical region. It does propose some challenges to the components in the heat pump cycle, mainly a robust and stable compressor, because of the typical operating pressures being 5-10 times higher than traditional heat

pumps. The pressure inside the evaporator is typically between 20 to 40 bar and 80 to 130 bar in the gas cooler during heat rejection [Zhang and Yamaguchi, 2021].

Another strong property of CO_2 is its ability to transfer heat in the gas cooling process. Figure 1.4 shows a normal subcritical VC cycle's heat rejection, which means in the condenser.

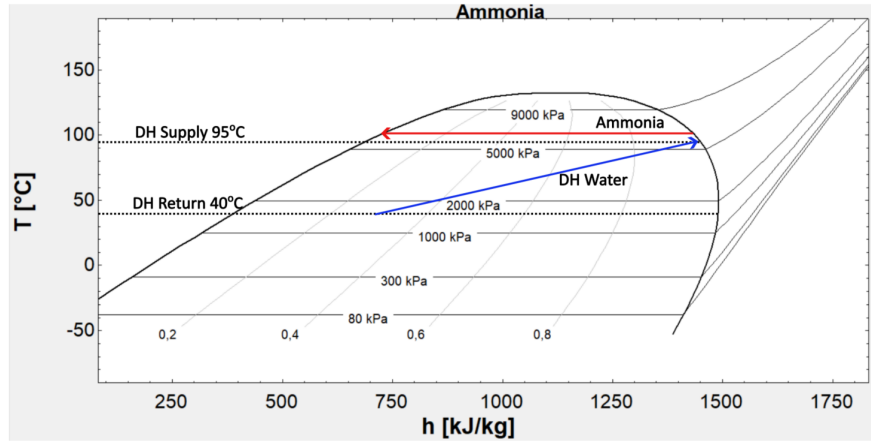


Figure 1.4: Sketch of temperature profiles and glides of the heat rejection process in a subcritical compression cycle with ammonia as the refrigerant.

It shows a water stream as the blue line and a refrigerant stream as the red line. The condensation happens at a constant temperature as the latent heat of condensation is utilised. The closest point between the two curves is called the pinch point or pinch temperature. It is desired to have the lowest possible pinch temperature, as this makes the most efficient heat transfer and therefore increases the COP. The pinch point in traditional VC cycles is usually located near the desuperheating side at the inlet to the condenser. The water inlet temperature also has an influence on how close the two curves can operate to each other [Danfoss, 2023].

Figure 1.5 shows a heat transfer process in the gas cooler of a TC cycle with CO_2 .

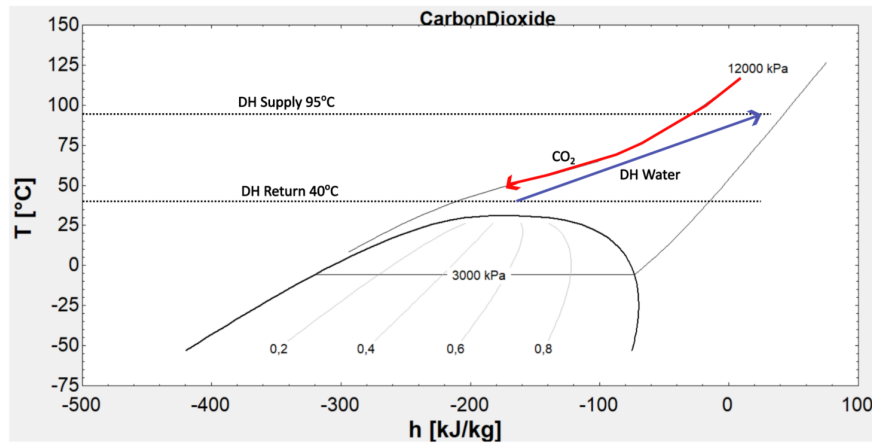


Figure 1.5: Sketch of temperature profiles and glides of the heat rejection process in a transcritical cycle with CO_2 as the refrigerant. CO_2 is at a pressure of 120 Bar.

As mentioned, this process does not compare with the normal condensation as the temperature is not constant and instead has a distinct glide. The glide matches the glide of water heating much better and the pinch point can be located in the middle or at the end of the section of the gas cooler. This brings an even higher influence on the water inlet temperature, which will dictate the gas cooling pressure [Danfoss, 2023] [Zhang and Yamaguchi, 2021].

One of the most critical and challenging characteristics of supercritical fluids near or at the supercritical state is their transport and thermodynamic properties, which change rapidly with only minor changes in temperature at a certain pressure. These are also sometimes referred to as the pseudo-critical points [Zhang and Yamaguchi, 2021]. Supercritical CO_2 also experiences changes in other properties like density, Prandtl number, thermal conductivity and dynamic viscosity. This poses a challenge, especially for the gas cooler, where a local spike or fall in the specific heat capacity or the Prandtl number can enhance or suppress heat transfer. Thermodynamic and transport properties for CO_2 at a wide range of temperature and pressure are shown in Figures 1.6a, 1.6b, 1.6c, 1.6d and 1.7. The data are extracted from EES, which uses the reduced Helmholtz model by [Span and Wagner, 2002]. Refpropm and CoolProp use the complete Helmholtz model with minor deviations from the reduced.

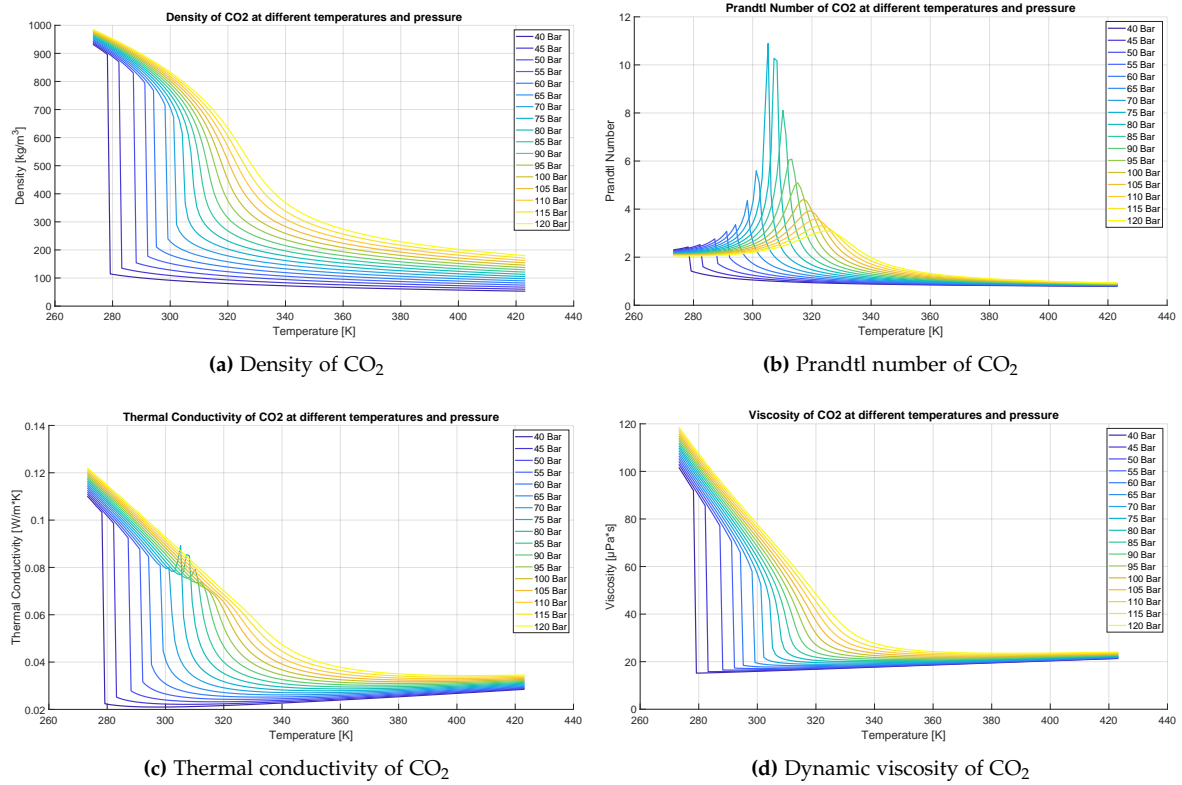


Figure 1.6: Transport and thermodynamic properties of CO₂ across a wide range of pressures and temperatures, covering sub-critical, near-critical, and super-critical regions.

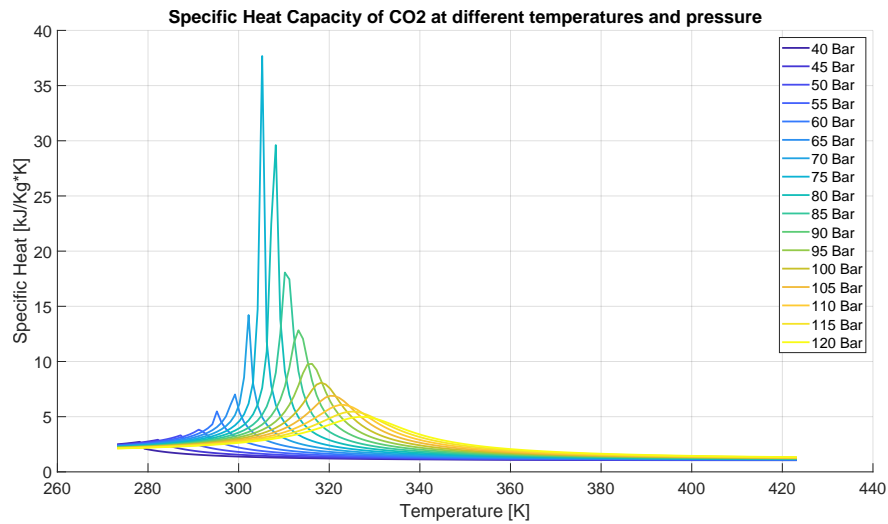


Figure 1.7: Specific heat capacity of CO₂

The figures show steep gradients in density and viscosity and spikes in the Prandtl number and specific heat around the critical point. It also shows that as the pressure increases, the temperature at which these spikes occur increases and their bandwidth widens. The peaks or dips become softer with high pressures and almost become flat at a pressure of 120 Bar, which is used in the high-pressure region for the heat pump at Aalborg Forsyning.

Another observation is that at sub-critical pressures, there is a discontinuity in some of the properties through the saturation line - one for vapour and one for liquid. On the contrary, at supercritical pressure, the fluid is considered to be single-phase, hence the continuity and no sudden 'jumps'.

The drastic changes in the thermophysical properties can have an impact on the heat transfer within the evaporator and gas cooler. Steep gradients in axial or radial density due to heating or cooling can result in buoyancy and/or flow acceleration effects, which may lead to enhancement or deterioration of heat transfer. On the other hand, a spike in Prandtl number or specific heat capacity could increase the heat transfer coefficient, however, close monitoring of the pressure will be necessary. These effects are not predicted well by correlations or models for the single-phase state, and will not be investigated further in this thesis [Zhang and Yamaguchi, 2021].

Chapter 2

Problem Statement

The objective of this master's thesis is to investigate the Transcritical CO₂ heat pump at Aalborg Forsyning and the surrounding system linked to the district heating network. The system is very dependent on source temperatures since the heat pump is a seawater heat pump with the evaporator in contact with the Limfjord Strait. The modelling will include steady-state and dynamic models with varying temperatures. Furthermore, a scenario where a stream of excess heat from the future PtX-facility Fjord PtX will be heat exchanged with the seawater from the Limfjord Strait will be modelled. The influence of the COP will be investigated. The system will include the modelling of a thermal stratified hot water storage tank. Lastly, a techno-economic feasibility analysis of a heat exchanger will be conducted to investigate if the gain in COP of the heat pump can make up for the implementation costs of such a heat exchanger.

2.1 Methodology

The first step is to analyse the existing district heating network in Aalborg with the new technologies that are being implemented. Since they are identical, the heat pump model will consist of one of the four modules. The heat pump will be modelled as transient with varying seawater temperatures of the inlet in the evaporator from the Limfjord Strait. The transcritical CO₂ heat pump consists of 4 components, which are each described and modelled individually. These are an evaporator, a compressor, a gas cooler and an expansion valve. The gas cooler and evaporator will be discretised into control volumes with the goal of obtaining their respective fluid properties with a high degree of accuracy. This is especially important in the gas cooler, as no condensation takes place and the temperature varies.

The dynamic model of the transcritical heat pump with and without a thermal stratified water tank is made to investigate the system's transient behaviour since heating demand and water inlet temperatures are time-dependent. To make the model easier in terms of computational time, it is split into so-called load points with intervals of 48 hours. There will be four load points in total, with the load points in the winter half-year being of higher detail since this is where the heat pump has the highest demand.

Chapter 3

Modeling

This chapter will be focused on describing the modelling parts of this master's thesis. The model will try to replicate the state-of-the-art TC CO₂ heat pump, starting with a steady-state model. Thereafter, a dynamic model with and without thermal storage.

In this thesis, the model will also investigate the heat pump's behaviour if the seawater's temperature to the evaporator's inlet is raised by heat exchange with excess heat from the future Fjord PtX system. The excess heat stream delivers between 29.8 and 51.6 MW at a temperature of 67°C [Aalborg Forsyning, 2025]. The heat exchanger will be modelled after the Effectiveness-NTU method.

3.1 System Breakdown and Topology

The district heating system considered in this thesis can be broken down into different subsystems. The topology of the entire system considered in this thesis is illustrated in Figure 3.1.

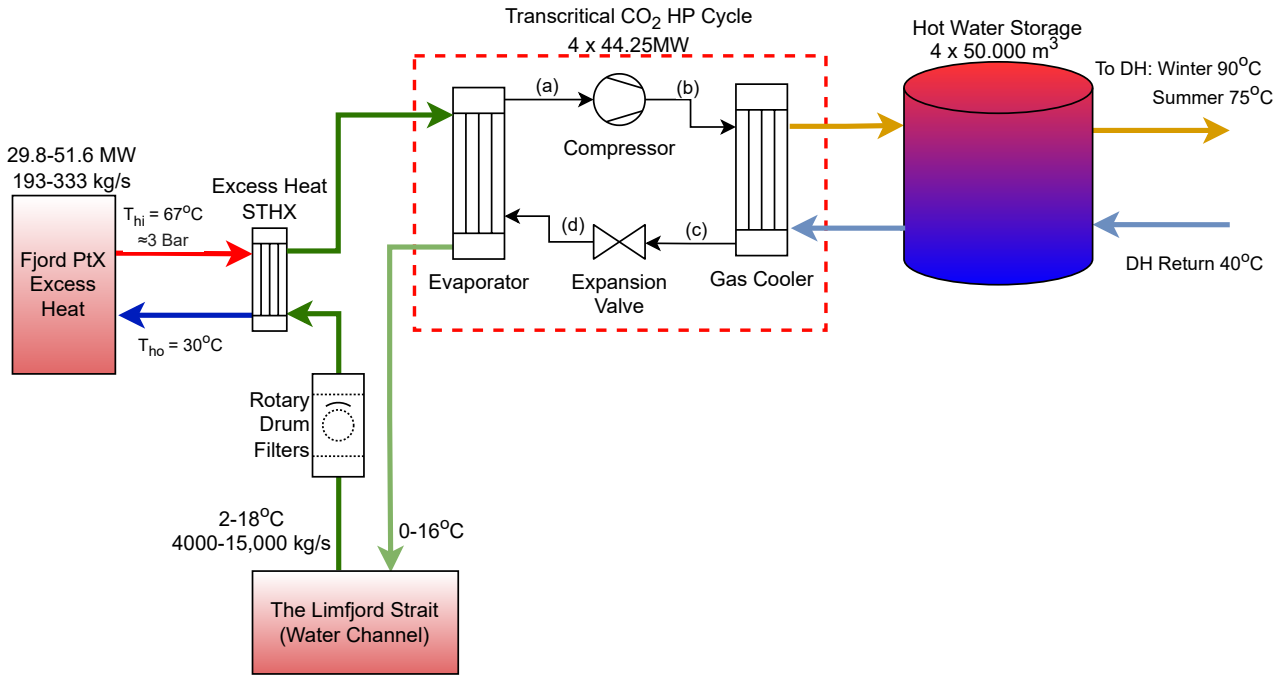


Figure 3.1: Topology of the system. Inspired by the future DHN in Aalborg and by Aalborg Forsyning.

There are several subsystems present, and the following section will break them down into individual streams. Starting from the left, excess heat from Fjord PtX in red and blue lines is present. The hot excess heat stream enters the heat exchanger, where it is heat exchanged with the cold seawater from the Limfjord Strait. The excess heat is returned by the blue stream to the PtX-facility again.

The other subsystem is presented with green lines. Seawater is pumped into a separate water channel that Aalborg Forsyning has access to. It goes through a rotary drum filter that cleans the water from seaweeds, fish, mussels, etc. This project does not consider the drum, which is only indicated on the topology. The seawater enters the heat exchanger, where heat from Fjord PtX is transferred. After the heat is exchanged, the stream flows to the evaporator, which works as the TC HP's heat sink. The return from the evaporator is going back into the Limfjord Strait.

The heat pump cycle will be elaborated in detail later in this chapter.

The next subsystem consists of the light blue and yellow lines. It resembles the auxiliary system to help deliver the district heating demand and handle the return, represented by a thermal energy storage. The thermal energy storage is made up of four 50,000 m^3 hot water storage tanks. In this thesis, only one tank is modelled for simplicity.

The outlet from the gas cooler is sent to the top layer in the storage tank and cold water from the bottom layer is sent back to the gas cooler inlet at 40°. On the other side of the hot water storage tank, the district heating water is sent out to the DHN from the top layer at a temperature of either 90°C or 75°C, depending on the season. The district heating return water is sent into the bottom layer of the hot water storage tank.

3.2 Steady-State Transcritical Heat Pump Model

The heat pump at Aalborg Forsyning has a heating capacity of 177 MW with a compressor power of 59 MW. The heat pump is made up of 4 equally sized heat pumps. They are not made in any connection with each other, ie, in series, in parallel or in cascade. They can run independently of each other, and therefore, in the current model, it is selected to model just one heat pump of 44.25 MW heating capacity with a compressor power of 14.75 MW. The heat pump will be the main focus of this thesis and most of the efforts will be put into modelling this and understanding the parameters and their behaviour.

The component designs will try to replicate the heat pump currently being implemented at Aalborg Forsyning, providing precise and accurate descriptions of the system and its results.

The water side of the heat pump model, both in the evaporator and gas cooler, will have constant inlet and outlet temperatures and mass flows. A sketch of the steady-state heat pump is seen in Figure 3.2.

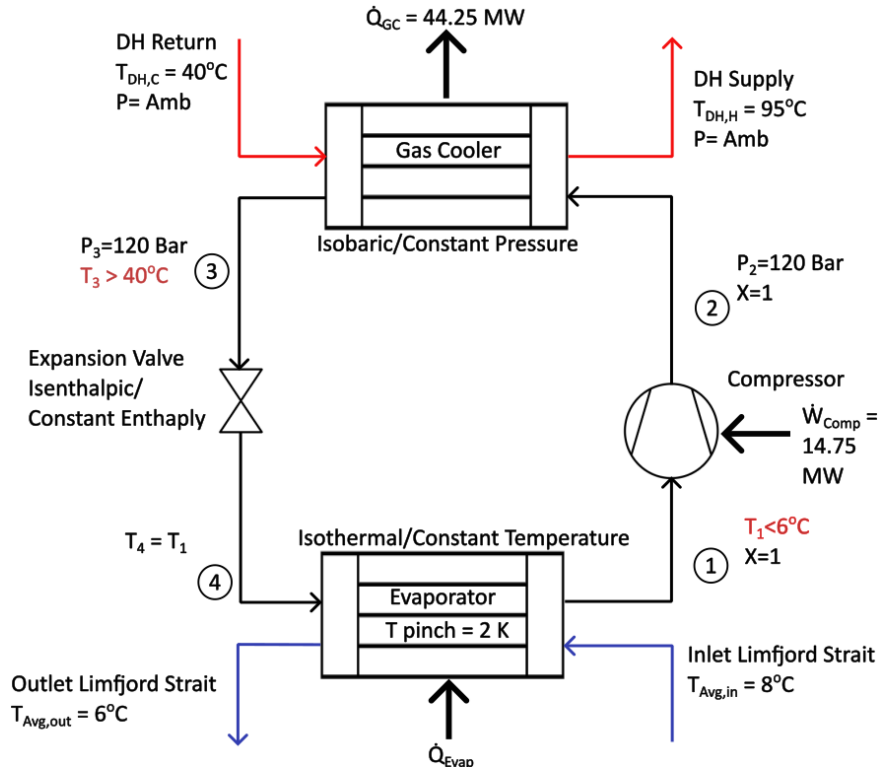


Figure 3.2: Sketch of Steady State Heat Pump Model

The model is limited by the two heat exchangers ie. the evaporator and the gas cooler. The temperature curves of the two streams cannot cross, as this would be against the 2nd law of thermodynamics. Therefore, the temperature of the refrigerant out of the evaporator has to be lower than the inlet temperature of the Limfjord Strait (6°C/281 K). Likewise, the temperature of the refrigerant leaving the gas cooler has to be higher than the DH return temperature (40°C/313 K).

The isentropic efficiency of the compressor is assumed to be 0.85. The expansion valve is modelled as isenthalpic.

The gas cooler and evaporator are modelled as shell-and-tube counterflow heat exchangers. The overall heat transfer coefficient (U-value) of both the gas cooler and the evaporator is estimated to be $700 \frac{W}{m^2 \cdot K}$. The U-value has a typical range between 300 and $1200 \frac{W}{m^2 \cdot K}$ [VDI, 2010].

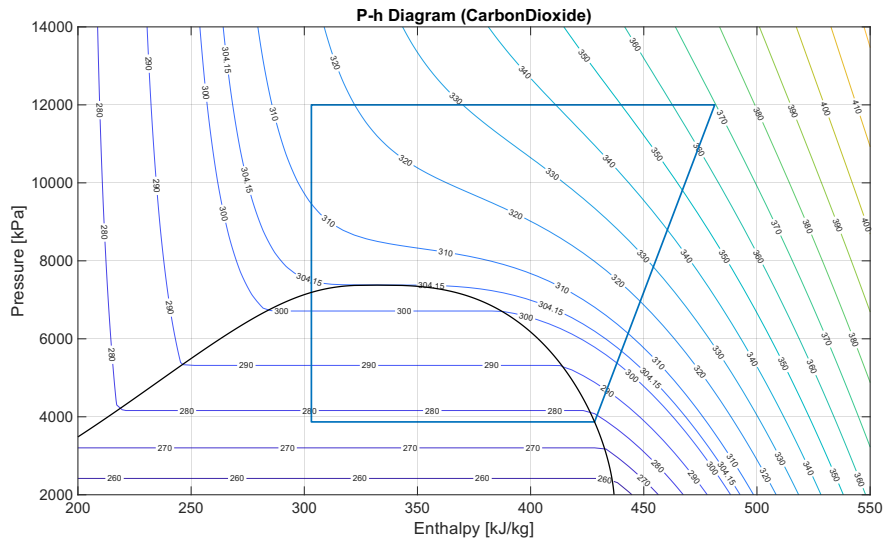


Figure 3.3: P-h diagram for the steady-state transcritical heat pump cycle.

The heat rejected in the gas cooler should be the same as the heat obtained from the Limfjord Strait and the power input from the compressor. The operating pressures are set to 120 bar on the high-pressure side and the resulting low-side pressure is 38.7 bar. The log P-h diagram of the steady-state TC heat pump cycle is seen in Figure 3.3.

In practice, a superheating of the vapour after the evaporator would be best suited to ensure that only vapour enters the compressor. This could be done with an internal heat exchanger where you draw energy from the gas cooling process before the expansion. The mass flow rates of each loop can be calculated. The loops are the cold and hot sides and the refrigerant loop. The mass flow of the refrigerant loop is calculated from the heating capacity and the work in the compressor from the enthalpy changes before and after the compressor stage.

The COP of the steady-state HP is calculated to be 3.35. The model is steady-state, yet plotting COP during the year is seen in Figure 3.4.

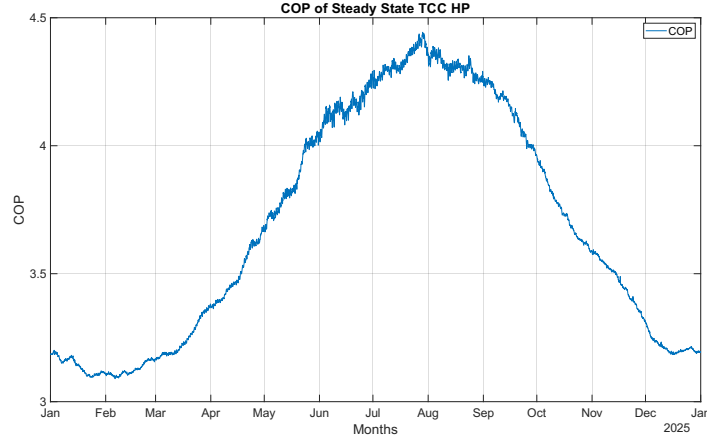


Figure 3.4: COP as a function of time.

The tendency of the COP corresponds to that of the seawater temperature. In the summer half-year, the heat pump is set to run the least even though it is suggested to be the most efficient at that period.

The UA-value of the gas cooler can be estimated with the *Logarithmic Mean Temperature Difference* (T_{LMTD}) seen in Equation (3.1) and (3.2).

$$T_{LMTD} = \frac{(T_{GC,in} - T_{DH,C}) - (T_{DH,H} - T_{GC,out})}{\log\left(\frac{T_{GC,in} - T_{DH,C}}{T_{DH,H} - T_{GC,out}}\right)} \quad (3.1)$$

$$UA_{GC} = \frac{\dot{Q}_{GC}}{T_{LMTD}} \quad (3.2)$$

This is only supposed to act as a starting guess for the dynamic model. The resulting UA value in the gas cooler is $3.23 \cdot 10^6$ [W/K]. Future UA-values for the evaporator and gas cooler in the dynamic model will be presented accordingly.

It is worth noting that the 4 heat pumps are not connected in any way, as already mentioned. Heat pumps connected in series or cascade could potentially and most likely increase the overall COP.

3.3 Heat Exchanger Model for Excess Heat from Fjord PtX

A *Heat Exchanger* (HX) is a device that facilitates the heat exchange between two fluids with different temperatures and possibly other conditions, while keeping them separated. This section will give an overview of the modelling of a water-to-water heat exchanger unit that will be placed before the cold storage.

The excess heat coming from Fjord PtX, which has to be heat exchanged, is estimated to be between 29.8 and 51.6 MW at a temperature of 67°C. The heat delivery is not constant and is estimated to fluctuate within the mentioned range. The heat delivery from Fjord PtX is seen in Figure 3.5a and 3.5b.

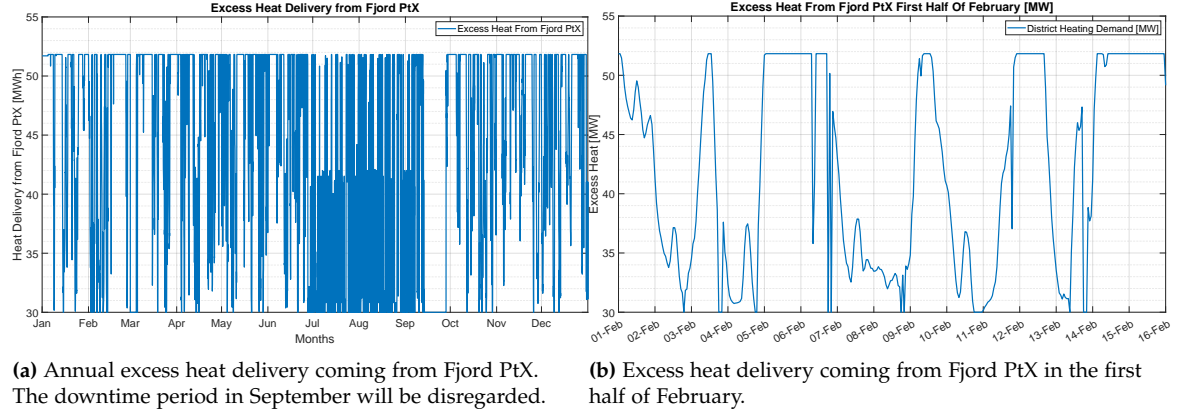


Figure 3.5: The figures above show the excess heat delivery from Fjord PtX to Aalborg Forsyning for each hour, and for the first half of February the same year [Aalborg Forsyning, 2025]

The excess heat from Fjord PtX will arrive at a temperature of 67°C and can be cooled down to 30°C. Therefore, it is only the mass flow rate that changes whenever the heat delivery changes, which it does frequently. The period from mid-September to end-September suggests some downtime period; this could be where maintenance is planned. The close-up in Figure 3.5b indicates that there is no specific tendency or structure of the heat delivery. It could indicate that the simulation is based on electricity prices or some other factor that has extreme fluctuations.

The mass flow rate can be determined from the sensible heat transfer equation for a flowing fluid seen in Equation (3.3).

$$\dot{Q} = \dot{m} \cdot c_p \cdot \Delta T \quad (3.3)$$

Where \dot{m} [kg/s] is the mass flow rate.

An innovative type of heat exchanger is the so-called plate-and-frame heat exchanger, or just plate heat exchanger, which consists of a series of plates with corrugated flat flow passages [Yunus A. et al., 2016]. The hot and cold fluid flows in an alternate direction, and each fluid flow is surrounded by a plate of the opposite fluid, resulting in efficient heat transfer. Another type, and probably the most common one, is the shell-and-tube heat exchanger. A *Shell-and-Tube Heat Exchanger* (STHX) consists of tubes packed in a shell with its axis parallel to the tubes. Baffles inside the shell are made to guide the shell side fluid through the shell. The other fluid flows through the shell within tubes. They vary in terms

of the number of passes within the tube and shell. The more passes, the higher the heat transfer, but also the cost increases, as well as the pressure drop.

Both plate HXs and STHXs work well with the two fluids are water, however, plate HXs cannot handle large pressure drops [Yunus A. et al., 2016]. In this case, both streams are at low pressure (below 10 bar). The HX in this scenario, with the excess heat from Fjord PtX, is modelled as an STHX with one shell pass and two tube passes. The excess heat scenario and STHX is sketched in Figure 3.6.

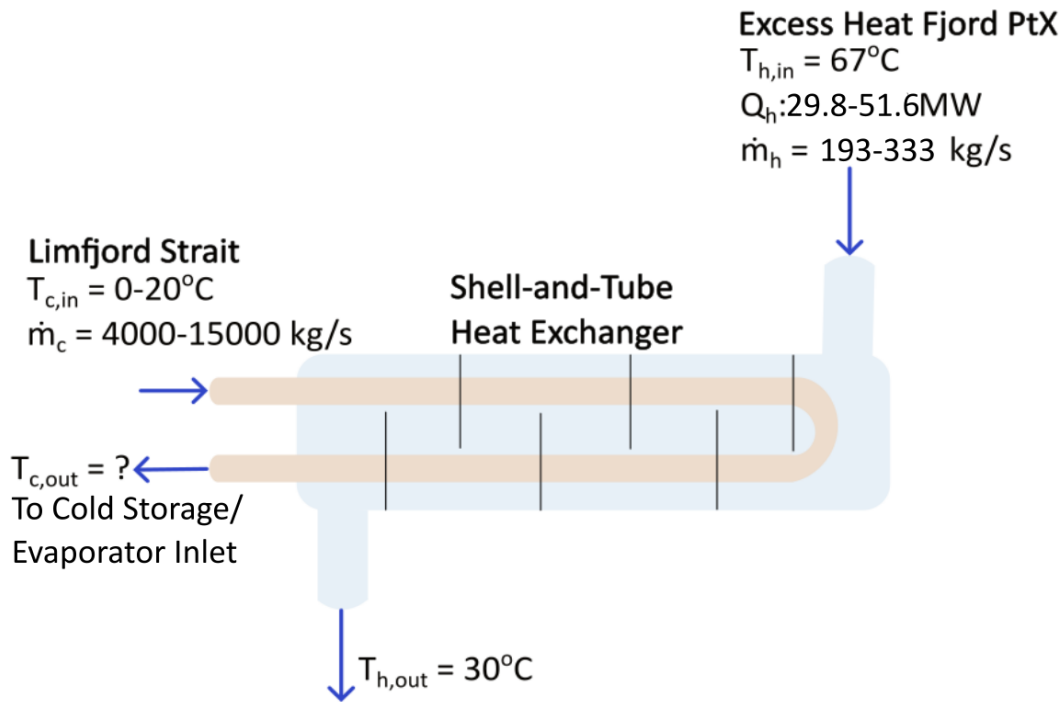


Figure 3.6: Illustration of the STHX used for the excess heat scenario.

As it is evident that the cold stream, T_c , from the Limfjord Strait that has to be heated by the excess heat from Fjord PtX, has a very high flow rate compared to the excess heat stream. The flow rate of T_c is between 12 and 77 times higher than T_h based on the given circumstances. This poses a challenge when designing the HX and choosing the type of HX. STHXs are generally more robust and reliable, which is a good feature in this scenario where seawater comes in at such a high volume flow rate [Yunus A. et al., 2016]. In terms of the pressures of the two streams, a plate heat exchanger could also be an option.

The STHX is designed using the Effectiveness-NTU (ϵ -NTU) method according to [VDI, 2010] and [Yunus A. et al., 2016] [Sanford and Gregory, 2009]. When the outlet temperature of one or more of the fluids is unknown, this is the preferred method over the LMTD method,

which would require iterations. The STHX should be modelled after the 'worst' case scenario, so this is when there is the highest flow rate from the Limfjord Strait and the lowest flow rate of Fjord PtX. The effectiveness of the heat transfer is calculated with Equation (3.4).

$$\varepsilon = \frac{\dot{Q}}{Q_{\max}} = \frac{\text{Actual heat transfer rate}}{\text{Maximum possible heat transfer rate}} \quad (3.4)$$

The actual heat transfer rate in the STHX can be determined from the energy balance in Equation (3.5).

$$\dot{Q} = C_c \cdot (T_{c,\text{out}} - T_{c,\text{in}}) = C_h \cdot (T_{h,\text{out}} - T_{h,\text{in}}) \quad (3.5)$$

Where $C_c = \dot{m}_c \cdot c_p$ and $C_h = \dot{m}_h \cdot c_p$ are the heat capacity rates of the cold and hot fluid, respectively. The ratio between the minimum and maximum heat capacity is denoted as the capacity ratio C_R , as seen in Equation (3.6).

$$C_R = \frac{C_{\min}}{C_{\max}} \quad (3.6)$$

Next, to determine the maximum amount of heat transfer possible, the highest temperature difference between the two streams is found in Equation (3.7).

$$\Delta T_{\max} = T_{h,\text{in}} - T_{c,\text{in}} = 67 - 0 = 67^\circ\text{C} \quad (3.7)$$

Since both streams are considered to be water, the difference in heat capacity rates depends on the mass flows. The maximum possible heat transfer rate in the heat exchanger is then determined in Equation (3.8).

$$\dot{Q}_{\max} = C_{\min} \cdot (T_{h,\text{in}} - T_{c,\text{in}}) \quad (3.8)$$

Where C_{\min} is the smallest of the two heat capacity rates and therefore the limiting of the two. The *Number of Transfer Units* (NTU) is determined in Equation (3.9).

$$\text{NTU} = \frac{UA_s}{C_{\min}} = \frac{UA_s}{(\dot{m} \cdot c_p)_{\min}} \quad (3.9)$$

Which is a dimensionless number. The larger the NTU, the larger the heat exchanger, since NTU is proportional to A_s . It can be shown that the effectiveness of a heat exchanger depends on the NTU and the capacity ratio, C_R . Below in Equations (3.10) and (3.11), the relations for an STHX with two tube passes are shown.

$$\text{NTU} = -\frac{1}{\sqrt{1 + C_R^2}} \ln \left(\frac{2/\varepsilon - 1 - C_R - \sqrt{1 + C_R^2}}{2/\varepsilon - 1 - C_R + \sqrt{1 + C_R^2}} \right) \quad (3.10)$$

$$\varepsilon = 2 \left\{ \left(1 + C_R + \sqrt{1 + C_R^2} \right) \frac{1 + \exp \left(-NTU \sqrt{1 + C_R^2} \right)}{1 - \exp \left(-NTU \sqrt{1 + C_R^2} \right)} \right\}^{-1} \quad (3.11)$$

The effectiveness is a number between 0 and 1. It increases rapidly with low values of NTU but fades out at higher values of NTU, typically around 3. This means that an HX with a higher NTU and therefore larger size becomes economically expensive, since only a small increase in NTU leads to a small increase in effectiveness.

3.3.1 Heat Exchanger Dimensions

The heat exchanger area and length of the pipes inside the device can be determined based on the NTU from Equation (3.9). The length of the pipes can be determined if the piping diameter is known. The inner diameter of the seawater pipe is DN2000, so 2000 mm or 2 meters. This is, of course, the pipe for the seawater and not the pipe diameter from the excess heat, which is not known. The area of the STHX can be determined by Equation (3.12).

$$A_{STHX} = \frac{NTU \cdot C_{\min}}{U_{STHX}} \quad (3.12)$$

If evaluated for different scenarios, like in the current case, the highest value of A_{STHX} should be chosen. The length of the pipes inside the STHX can be determined with Equation (3.13).

$$L_{STHX} = \frac{A_{STHX, \text{Max}}}{\pi \cdot D_{\text{inner, pipe}}} \quad (3.13)$$

The dimensions of the STHX result in the following values from Table 3.1.

Table 3.1: Dimensions of the STHX analysis

Dimension	Value
$A_{STHX} [\text{m}^2]$	1438.7
$L_{STHX} [\text{m}]$	229
$\varepsilon [-]$	0.56-0.78
NTU [-]	0.82-0.96

The results of ε and NTU are moderate and not particularly high in terms of heat transfer capabilities.

3.3.2 Pressure Losses in the Heat Exchanger

Pressure losses are encountered in many practices, especially when the flow is turbulent, as it is in the case of the STHX. The friction factor in a fully developed turbulent pipe flow depends on the *Reynolds number* (Re) and the relative roughness of the pipe, which is a ratio between the roughness of the pipe and the pipe diameter ϵ/D . The roughness of 0.15 mm for galvanised steel is used.

The pressure loss can be determined by the Darcy-Weisbach equation seen in Equation (3.14).

$$\Delta P = f \cdot \frac{L}{D} \cdot \frac{\rho V^2}{2} \quad (3.14)$$

Where ΔP is the pressure loss, friction factor, L is the length of the pipe, D is the diameter of the pipe, ρ is the fluid density, and V is the average fluid velocity.

The friction factor can be found using the implicit Colebrook equation seen in Equation (3.15).

$$\frac{1}{\sqrt{f}} = -2.0 \log_{10} \left(\frac{\epsilon/D}{3.7} + \frac{2.51}{\text{Re} \sqrt{f}} \right) \quad (3.15)$$

With such high mass flows, in the cold stream from the Limfjord Strait, the pressure losses from minor losses due to bends, elbows, etc., should also be considered. These depend on representative loss coefficients. The loss coefficient for a 180-degree bend should be considered, which is 0.3 when regarded as flanged [Yunus A. et al., 2016]. The minor pressure loss can be expressed as in the following Equation (3.16).

$$\Delta P_{\text{minor}} = K_L \cdot \frac{\rho \cdot V^2}{2} \quad (3.16)$$

Where K_L is the loss coefficient. The power the pump has to deliver to overcome these pressure losses can be determined as in Equation (3.17)

$$\dot{W}_{\text{pump}} = \dot{V} \cdot \underbrace{(\Delta P + \Delta P_{\text{minor}})}_{\text{Total Pressure Loss}} \quad (3.17)$$

Where $\dot{V}[m^3/s]$ is the volume flow rate.

3.4 Dynamic Model of District Heating System

For the dynamic model of the HP system to work, some data gathering has to be made. The seawater temperature of the Limfjord Strait has been shown in Figure 1.2. The average temperature will be used throughout the analysis. For the heat pump model, the modelling will be split into so-called *Load Points* (LPs), where there are four different ones referring to different periods/seasons. The LPs are seen below in Table 3.2.

Table 3.2: Heat pump plant annual operating hours, load points and supply and return temperatures. [Aalborg Forsyning, 2025]

Load Points LP	Months	Seawater Temp °C	Supply Temp °C	Return Temp °C	Full Load Hours/Year
1	Dec, Jan, Feb	3	90	38	1600
2	Mar, Apr, Nov	6	90	38	1200
3	May, Sep, Oct	9	90	40	800
4	Jun, Jul, Aug	15	75	40	400
Total					4000

The main focus is to model LP1 and LP2, as these are the periods with the highest demand and full load hours. Aalborg Forsyning estimates that the heat pump will be shut down completely for the warmest 5 months, so large periods of LP3 and LP4.

The demand for district heating varies throughout the year. In fact, this is one of the variables that varies the most. In a place like Denmark, the heating season is dominant in the winter half-year and almost non-existent during the summer. The demand for district heating over a whole year and a two-day period in LP1 from Aalborg Forsyning is shown in Figure 3.7a and 3.7b.

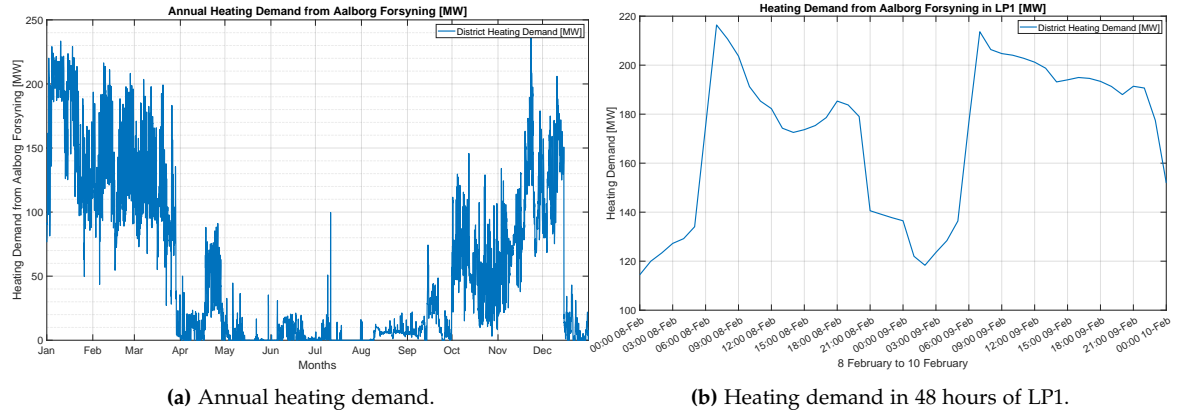


Figure 3.7: The figures above show the heating demand for Aalborg Forsyning for each hour, throughout 2024, and for two selected days during February the same year ie. in the LP1 period. The data is from 2024. [Aalborg Forsyning, 2025]

It is seen that demand is highest during the cold months, and it gets a characteristic curve-like shape. In December, there was a period when NJV3 were out of order, which explains the period with low heat delivery. This period will be disregarded, and if a model for the period is needed, data could be interpolated.

For the future dynamic pump model, the two-day period in February is used as LP1 reference for the demand. It is seen that during the day, there are peak hours in the morning and afternoon and low-demand periods during the night. At the peak periods, the demand is higher than can be supplied by the heat pumps, and therefore, a supplemental heat source has to be considered. This will be presented as the Hot Water Storage later in this thesis.

The supply and return temperatures of the district heating water can be seen in Figure 3.8.

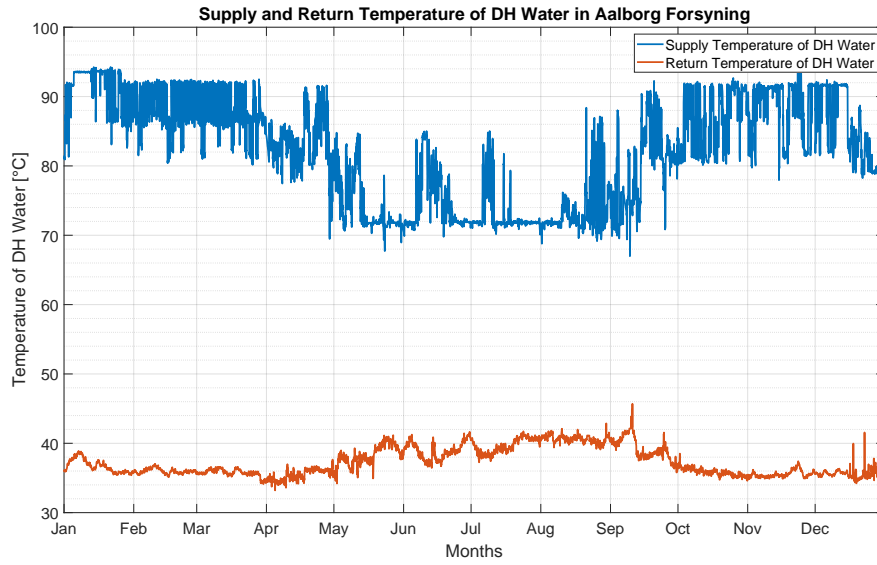


Figure 3.8: Supply and return temperature of the district heating water to and from Aalborg Forsyning. [Aalborg Forsyning, 2025]

The supply temperature is around 90°C from September to May and around 75°C in the Summer. The return temperature is more constant, with it being around 38°C from November to April and 40°C from May to October. This corresponds with the values from Table 3.2, which will be used in the modelling.

3.4.1 Discretisation of Gas Cooler and Evaporator

The heat exchangers, ie, gas cooler and evaporator, have been discretised into small sub-elements. By doing this, the properties of the fluid inside each control volume can be found, thus increasing the overall accuracy of the model. This is especially important in the gas cooler as it is a highly independent process. As mentioned in Section 1.4, supercritical CO₂ behaves differently from subcritical refrigerant. A gas cooler cools the supercritical CO₂ isobarically without phase change rather than an isothermal condensation. Figure 3.9 shows the spatial discretisation of the gas cooler with finite volumes.

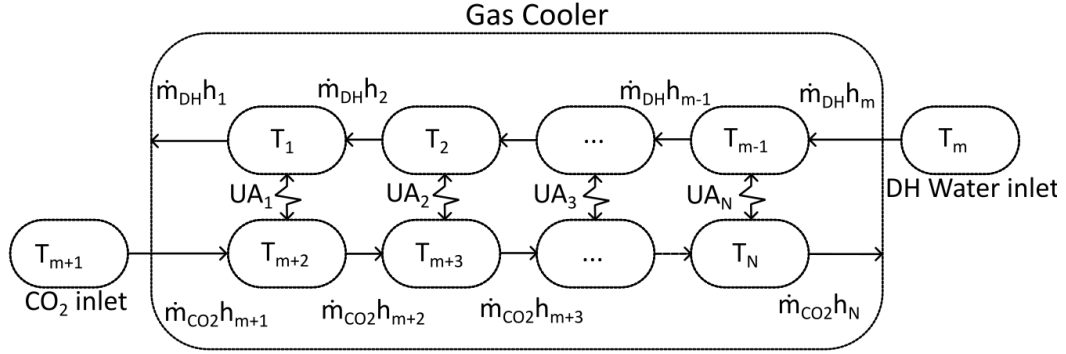


Figure 3.9: Spatial discretisation of the gas cooler. Discretisation inspired by [Holten et al., 2012] and [Nielsen and Sørensen, 2020].

The gas cooler is divided into N finite volumes and the total number of divisions is halved for each flow direction i.e.. $m = \frac{N}{2}$. The control volumes on each side, T_{m+1} and T_m , act as boundary conditions to satisfy the equation. The control volumes are assumed to be lumped, where the temperature within the control volume is assumed to be uniform at any given time during heat transfer.

The same discretisation scheme applies for the evaporator, with the difference being that the water inlet does not come from the district heating side but from the cold source side, i.e., the Limfjord Strait.

3.4.2 Conservation of Energy and Mass

The first law of thermodynamics, alongside the continuity equation, is used in the heat exchangers, neglecting changes in kinetic and potential energy as well as heat losses to the surroundings, stating that the heat exchangers are adiabatic. The energy balance equation for an open system/control volume is seen in Equation (3.18).

$$\sum_{i=1}^{\text{Inlets}} \dot{m}_{\text{in},i} \left(h_{\text{in},i} + \frac{1}{2} v_{\text{in},i}^2 + g z_{\text{in},i} \right) = \sum_{i=1}^{\text{Outlets}} \dot{m}_{\text{out},i} \left(h_{\text{out},i} + \frac{1}{2} v_{\text{out},i}^2 + g z_{\text{out},i} \right) + \left(\sum_{i=1}^{\text{Work In/outputs}} W_i + \sum_{i=1}^{\text{Heat transfer In/outputs}} Q_i \right) + \frac{dU}{dt} + \frac{dE_{\text{kin}}}{dt} + \frac{dE_{\text{pot}}}{dt} \quad (3.18)$$

The temperature is not a representative term to use since it changes during the length of the heat transfer in the gas cooler and stays constant in the evaporator. The axial conduction has also been left out due to the convective heat transfer being more dominant. Therefore, the terms have been rewritten to include specific enthalpies in Equations (3.19) and (3.20), which have been semi-discretized with respect to Figure 3.9 and treated with Upwind and Downwind discretization schemes to account for the flow direction

[Nielsen and Sørensen, 2020]. The two equations describe the changes in enthalpies in the DH cycle and refrigerant cycle, respectively.

$$V_{HS} \cdot \rho_i \cdot \frac{dh_i}{dt} = \rho_i \cdot A_{HS} \cdot u_i (h_{i+1} - h_i) + UA_i (T_{i+m+1} - T_i) \quad (3.19)$$

$$V_{CO2} \cdot \rho_{i+m+1} \frac{dh_{i+m+1}}{dt} = \rho_{i+m+1} \cdot A_{CO2} \cdot u_{i+m+1} (h_{i+m} - h_{i+m+1}) + UA_i (T_i - T_{i+m+1}) \quad (3.20)$$

Where $V[m^3]$ is the volume of each element, $UA_i[\frac{W}{K}]$ is the overall heat conductance for the current element, which is the product of the overall heat transfer coefficient and the heat transfer surface area, h is the specific enthalpy and u is the velocity of the fluid. On the right-hand side, $\rho \cdot A \cdot u$ equals the mass flow of the district heating water and refrigerant, respectively.

The return temperature and pressure of the district heating water provide the inlet conditions to the water side in the gas cooler, and the outlet of the compressor provides the inlet conditions of the refrigerant.

Mass

The mass flow rate is constant through the gas cooler and evaporator, which means that mass is also conserved from the inlet to the outlet.

$$\frac{dm}{dt} = \dot{m}_{in} - \dot{m}_{out} = 0 \quad (3.21)$$

This also means that mass is conserved between each sub-element in the control volume.

3.4.3 Solver and Indexing in Matlab

The dynamic modelling of the heat pump in MATLAB is inspired by a previous semester project from [Holten et al., 2012] and an internal research report from [Nielsen and Sørensen, 2020].

The modelling and discretization of the heat pump with or without thermal storage(s) consists of a mix of *Algebraic Equations* (AEs) and *Ordinary Differential Equations* (ODEs), which are combined into a coupled non-linear *Differential-Algebraic system of Equations* (DAE)-system. MATLAB has built-in solvers for these kinds of problems. The ode15s and ode23t solvers can solve index-1 linearly implicit problems when using a singular mass matrix first. The mass matrix is written with binary values, 1 for ODEs and 0 for AEs. Both solvers are able to handle stiff problems and can meet the requirements; however, the ode15s solver is chosen over ode23t while it has a higher accuracy.

In order for ode15s to work, the DAE-system has to be rewritten into differential equations, which are then multiplied by the mass matrix M as seen in Equation (3.22).

$$M(t, y) \cdot \frac{dH}{dt} = f(t, y) \quad (3.22)$$

As mentioned, if M is 1, it reads an ODE and if M is 0, it reads an AE. The solver tolerances used were 10^{-3} for the relative tolerance and 10^{-6} for the absolute tolerance [Mathworks, 2025].

The indexing used for the matrix and also for post processing is proposed in Figure 3.10.

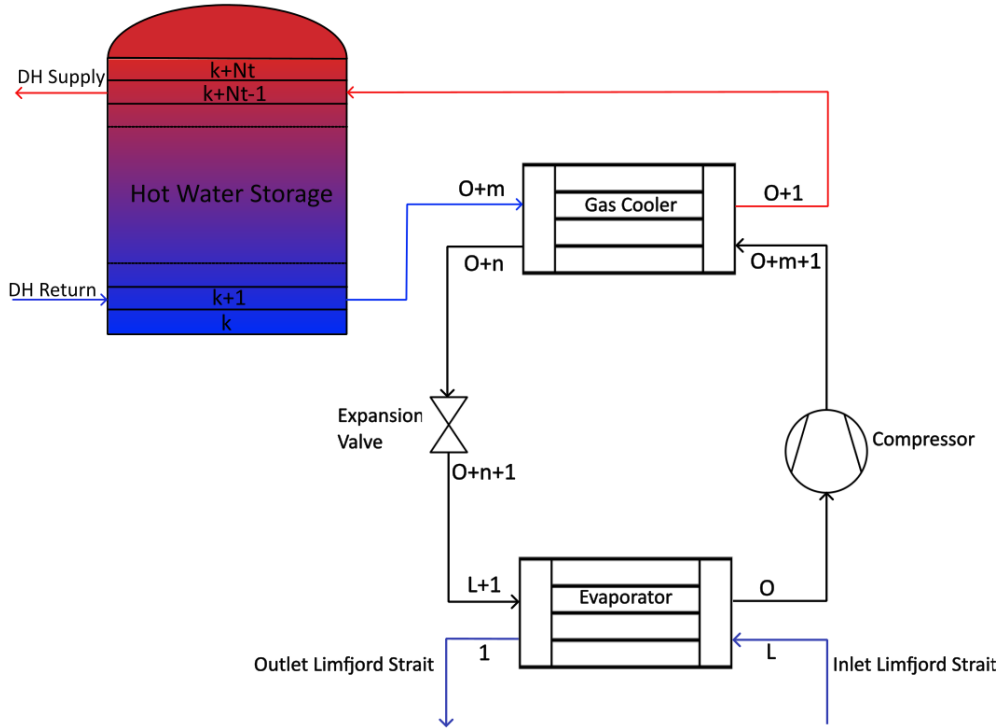


Figure 3.10: Indexing used in the Matlab model. Indexing inspired by [Holten et al., 2012] and [Nielsen and Sørensen, 2020].

The division of the two heat exchangers can be set up with the parameters o and n . The same can be set for the number of layers in the hot water storage connected between the district heating supply and return and the gas cooler. The number of layers is set by Nt . A grid independency study by [Holten et al., 2012] and [Nielsen and Sørensen, 2020] showed that a value of $N = 50$, i.e., 25 divisions in both evaporator and gas cooler in both directions, and $Nt = 250$ for the hot water storage, would be a reasonable parameter allowing for both high accuracy and low computational time.

3.5 Thermal Energy Storage

In this section, the modelling of the thermal energy storage will be elaborated. These will be included in some of the modelling to give better flexibility and can help in future 'sector coupling'.

The modelling of the thermal stratified water storage tank is based upon the article from [Kreuzinger et al., 2008]. Due to the storage tanks' larger volume and height, the velocity will become low, and axial heat conduction between the layers needs to be considered as well, unlike the heat exchangers. The thermal energy storage tank is compared to a convective-diffusive problem and is governed by the following PDE seen in Equation (3.23).

$$\rho c_p A_s \left[\frac{\partial T}{\partial t} + w \frac{\partial T}{\partial z} \right] = k A_s \frac{\partial^2 T}{\partial z^2} - h P (T - T_{amb}) \quad (3.23)$$

Where A is the cross-sectional area, w is the vertical flow velocity, T_{amb} is the ambient temperature of the surroundings, P is the circumference of the tank. The direction is seen as the vertical z -direction. The tank can be illustrated and discretised as in Figure 3.11 below.

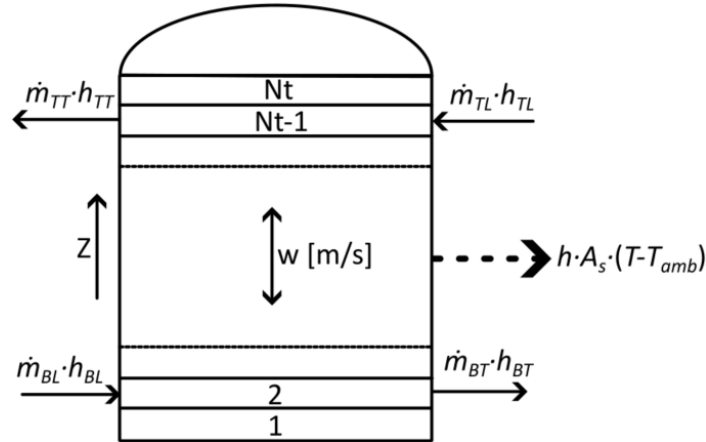


Figure 3.11: Stratified water storage tank with notation and discretisation. Inspired by [Kreuzinger et al., 2008].

Where the notations are TT - Top Tap, TL - Top Load, BL - Bottom Load and BT - Bottom Tap. The boundary conditions to the PDEs are located in Appendix A.1 with Equation (A.1) to (A.4). Nt is the number of finite volumes in the z -direction of the tank, which will be set at 250 [Holten et al., 2012] [Nielsen and Sørensen, 2020].

The solution to the PDE in Equation (3.23) can be found using a set of coupled ODEs with semi-discretisation. The discretisation scheme used is a so-called *Method of Lines* (MOA)

approach. If the fluid properties and temperatures are assumed constant over each finite volume, the following discretisation of the PDE in Equation (3.24) can be derived.

$$M_i c_p \frac{dT_i}{dt} = kA \frac{T_{i-1} - 2T_i + T_{i+1}}{dz^2} dz - \dot{m} c_p (T_{i-1/2} - T_{i+1/2}) - hA_s (T_i - T_a) \quad (3.24)$$

The discretisation scheme MOA can be divided into cell centres and cell faces as seen in Figure 3.12.

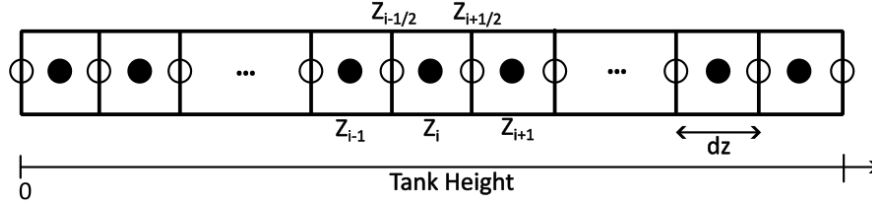


Figure 3.12: Finite volume discretization of the storage tank where • denotes cell centres and ○ denotes cell faces. [Kreuzinger et al., 2008]

The convective differentials must be formulated in terms of the flow direction, or numerical problems can occur. A positive flow direction $w > 0$ demands an upwind scheme and the downwind scheme is applied for a negative flow direction $w < 0$. This extra effort is done to the cell face temperatures $T_{i-1/2}$ and $T_{i+1/2}$ in the following Equations (3.25) and (3.26) [Kreuzinger et al., 2008].

$$w > 0 \begin{cases} T_{i-\frac{1}{2}} = T_{i-1} + \frac{\Phi^{i-\frac{1}{2}}}{2} (T_i - T_{i-1}) \\ T_{i+\frac{1}{2}} = T_i + \frac{\Phi^{i+\frac{1}{2}}}{2} (T_{i+1} - T_i) \end{cases} \quad (3.25)$$

$$w < 0 \begin{cases} T_{i-\frac{1}{2}} = T_i - \frac{\Phi^{i-\frac{1}{2}}}{2} (T_i - T_{i-1}) \\ T_{i+\frac{1}{2}} = T_{i+1} - \frac{\Phi^{i+\frac{1}{2}}}{2} (T_{i+1} - T_i) \end{cases} \quad (3.26)$$

Where Φ is the so-called flux limiter function. The numerator in the function, $\Phi^{i-\frac{1}{2}}$ and $\Phi^{i+\frac{1}{2}}$ determines which discretization scheme should be used. If both limiter functions are 0, the Upwind Scheme is used, if they are set to 1, the Central Difference Scheme is used and if they are set to 2, the Downwind Scheme is used. The Central Difference Scheme is very dependent on the resolution of the spatial discretisation. It is able to predict the diffusion term with high accuracy, even with a sharp gradient in the spatial profile. However, it will also lead to spatial oscillations. Therefore, a mix between the different schemes can result in an oscillation-free reconstruction with sharp transitions [Kreuzinger et al., 2008]. This can be done with the introduction of a shaping function, $\hat{\theta}$, which is defined in Equation (3.27) and (3.28).

$$w > 0 : \begin{cases} \hat{\theta}^{i-1/2} &= \frac{T_{i-1}-T_{i-2}}{T_i-T_{i-1}} \\ \hat{\theta}^{i+1/2} &= \frac{T_i-T_{i-1}}{T_{i+1}-T_i} \end{cases} \quad (3.27)$$

$$w < 0 : \begin{cases} \hat{\theta}^{i-1/2} &= \frac{T_{i+1}-T_i}{T_i-T_{i-1}} \\ \hat{\theta}^{i+1/2} &= \frac{T_{i+2}-T_{i+1}}{T_{i+1}-T_i} \end{cases} \quad (3.28)$$

Many different limiter functions exist and [Kreuzinger et al., 2008] has tested several. They found the Superbee limiter function to be the best in terms of reconstructing the sharp spatial transitions. The Superbee function is defined in Equation (3.29).

$$\Phi(\hat{\theta}) = \max(0, \min(1, 2\hat{\theta}), \min(2, \hat{\theta})) \quad (3.29)$$

The energy content in the storage tank can be calculated with Equation (3.30).

$$E_{\text{tank}} = m_{\text{water}} \cdot c_p \cdot T_{\text{avg}} \quad (3.30)$$

Where Q_{tank} is the energy content in the tank in Joules, m_{water} is the mass of water which can be calculated from the tank volume and density of water and T_{avg} is the average temperature of water in the tank.

Chapter 4

Results of Dynamic Transcritical Heat Pump Model and Heat Exchanger Model

This Chapter will present and discuss the results of the general dynamic TC HP model with and without thermal energy storage as presented in Section 3.4 and also the heat exchanger model with excess heat as presented in Section 3.3.

4.1 Dynamic Transcritical Heat Pump Model

The heat pump has been modelled to investigate the startup behaviour starting from the initial conditions. The heat pump is going from a standby state to full load condition. The initial conditions and other parameters used are as follows:

- Initial mass flow of CO₂ refrigerant: 1 kg/s
- Constant mass flow of seawater into the evaporator: 4000 kg/s
- Constant mass flow of district heating water into the gas cooler: 170 kg/s
- Initial temperature of district heating water: 40°C
- Constant temperature from Limfjord Strait: 2°C
- Initial refrigerant temperature in refrigerant cycle: 0°C
- Initial refrigerant pressure in refrigerant cycle: 1100 kPa
- $UA_{\text{Evaporator}} = 6566 \frac{\text{kW}}{\text{K}}$
- $UA_{\text{Gas Cooler}} = 6988 \frac{\text{kW}}{\text{K}}$

The UA values are provided by MAN Energy Solutions [Aalborg Forsyning, 2025].

A Ph-diagram showing the dynamic model is seen in Figure 4.1.

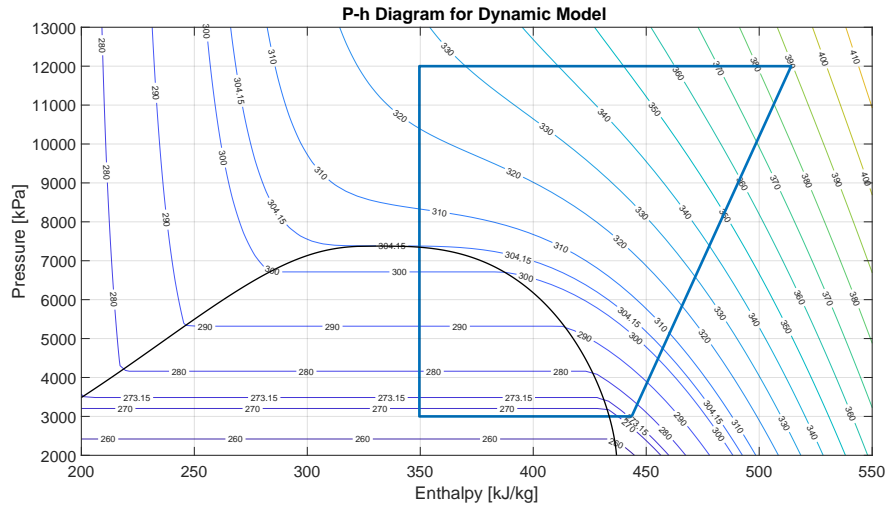


Figure 4.1: Ph-Diagram of the dynamic heat pump cycle

The resulting COP of the dynamic model is 2.33, which is significantly lower than the steady state model of 3.35, and is also significantly underestimated from what MAN provides. The dynamic model has lower heat transfer than the steady-state model in both the gas cooler and the evaporator. This suggests some tweaking should be done to the dynamic model.

The aforementioned distinct temperature glide in the gas cooler is seen in Figure 4.2. The temperature glide is shown as a function of the dimensionless gas cooler length.

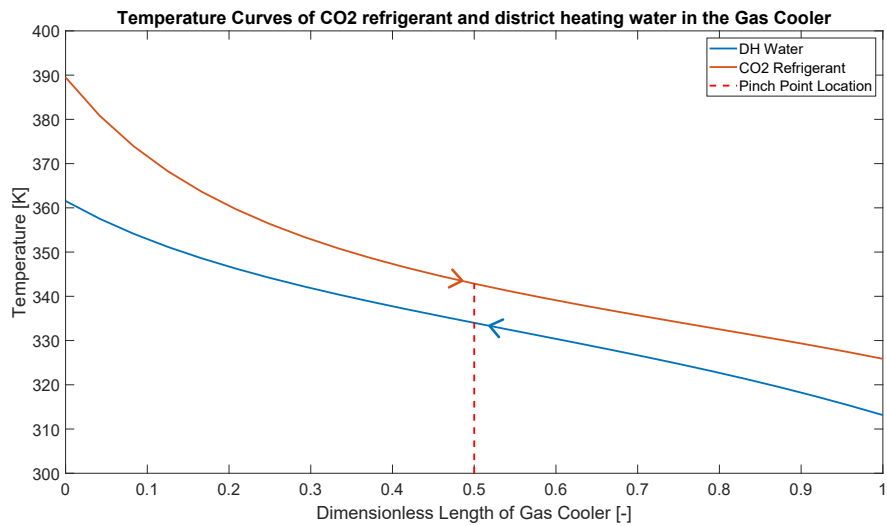


Figure 4.2: Temperature distribution curves in the gas cooler as a function of the dimensionless length of the gas cooler.

The orange curve shows the cooling of the CO₂ refrigerant from left to right and the blue curve shows the heating of the district heating water from right to left. The district heating water reaches a temperature of 361.5 [K], which is deemed sufficient for the DHN. It can be observed that the minimum temperature approach or pinch point is located in the middle of the gas cooler, which matches what was described in Section 1.4.

Likewise, the temperature curves for the evaporator are seen in Figure 4.3.

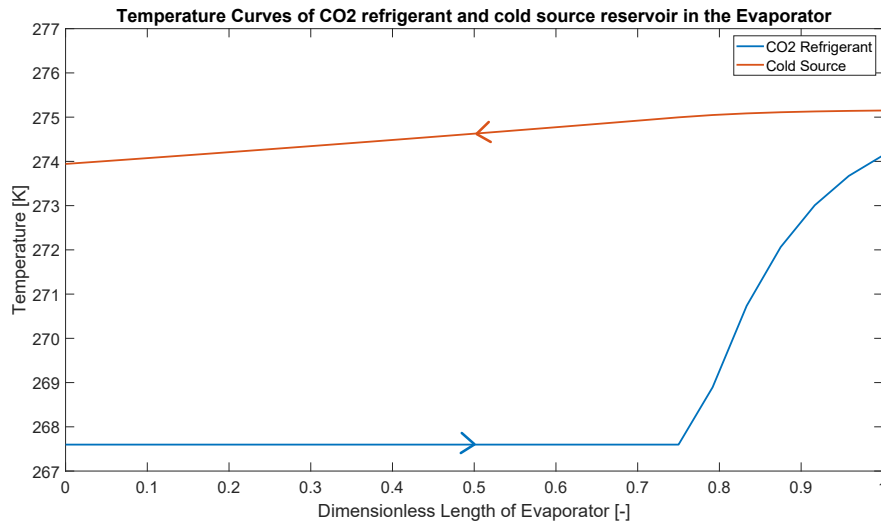


Figure 4.3: Temperature distribution curves in the evaporator as a function of the dimensionless length of the evaporator.

The blue curve shows the evaporation of the CO₂-refrigerant going from left to right, until approximately three-quarters of the evaporator length. Hereafter, there is a superheating of the CO₂-refrigerant as was also evident on the Ph-diagram in Figure 4.1. The cooling of the cold source ie. seawater from the Limfjord Strait, is seen as the orange curve from right to left.

The outlet temperature of the DH water is shown as a function of time in Figure 4.4. This is done to understand how the heat pump works from the 'idle/standby' condition to the full load condition.

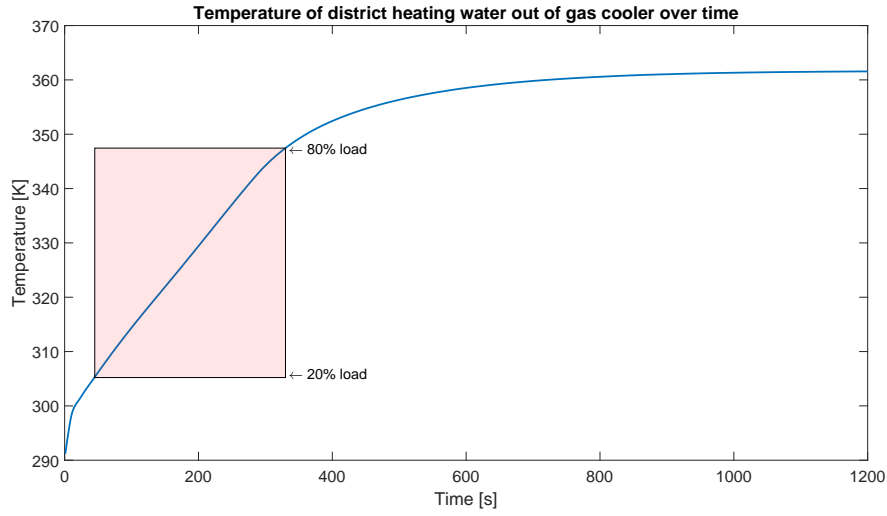


Figure 4.4: Dynamic start-up response of the district heating water temperature as a function of time.

It is seen that the temperature of the district heating water rises quickly in the beginning and then settles around 800 seconds and reaches steady-state at approximately 1000 seconds (16.67 minutes). The heat pump can manage to go from 20% to 80% load change in approximately 300 seconds (5 minutes). This is twice as fast as MAN has indicated in their tender documents [Aalborg Forsyning, 2025]. It shows a fast start-up time for the system, which could be a huge benefit when the electricity prices fluctuate. The faster startup time than what has been provided is likely due to differences in input conditions or the provider not wanting to overestimate the heat pump's performance.

It is observed from Figure 4.4 that the temperature of DH water out of the gas cooler rises immediately and during this ramp-up, there is no 'dead-time' or delay in the beginning. This is normally the case, and it is a consequence of thermal inertia, such as the gas cooler pipes and walls being cold at the start and needing some time to absorb heat before it can transfer it to the DH water. The other is compressor or refrigerant dynamics. The refrigerant cycle starts with a very low mass flow of 1 kg/s and needs time to settle and stabilise.

4.2 Results from Heat Exchanger Analysis

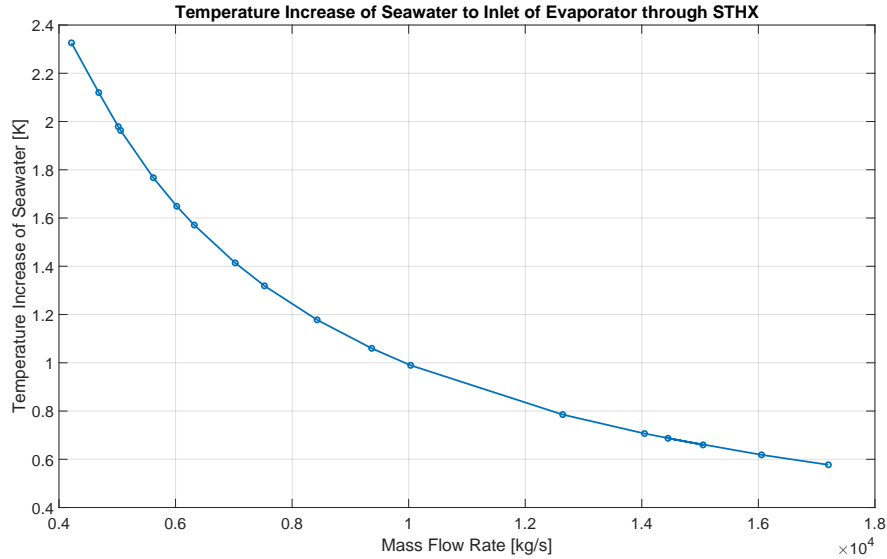
The inlet flow rate from the Limfjord Strait is dependent on the seawater temperature. The temperature difference (ΔT) is determined as follows in Table 4.1.

Table 4.1: Temperature differences used to calculate the mass flow of the seawater into the heat exchanger.

Range	ΔT
$T_{in} < 2^{\circ}\text{C}$	2
$2 \leq T_{in} < 3^{\circ}\text{C}$	3
$3 \leq T_{in} < 4^{\circ}\text{C}$	4
$T_{in} > 4^{\circ}\text{C}$	5

When the seawater temperature is under 2°C , the mass flow rate will be highest. As the temperature difference gets higher, the mass flow rate will become lower.

As the STHX will be placed before the heat pump, these high mass flow rates should be modelled within the STHX as well. Different flow rates, which relate to different pinch temperatures at COPs of 2.5, 3 and 3.5, are tested. The flow rate of the excess heat stream from Fjord PtX is constant in this scenario at 51.6 MW with a mass flow of 333 [kg/s]. The results are shown in Figure 4.5.

**Figure 4.5:** Temperature increase of the seawater to the inlet of the evaporator when heat is exchanged in the STHX.

This is calculated based on the entire heating capacity of the four heat pumps of 177 MW. The assumption is that the same tendency is present for one heat pump with a quarter of the mass flow.

It can be seen that the temperature increase is the highest at the lowest flow rates and has an exponential decay when subject to higher mass flow rates. At the highest mass flow rates, the seawater temperature only increases by around 0.6 K, which is insignificant. This

would mean that at the lowest seawater temperatures in the winter, the temperature increase due to the excess heat might still not be possible for the HP to operate, at least not in full load. Some days it would mean that the heat pump would be able to operate rather than being shut down completely and other times it would mean that the heat pump could operate in full load rather than part load.

Overall, it would mean that the heat pump's COP is higher, due to the smaller compressor work that is needed. This will be investigated later in Section 4.4.

The capacity ratio, C_R , is, as mentioned in Equation (3.6), the relationship between the heat capacity rates of the hot and cold fluid. In this scenario, the heat capacity ratio is very low and close to zero. Values of C_R vary between 0.0137 and 0.059, which indicates that $\dot{C}_c \gg \dot{C}_h$. This means that the temperature increase of the cold fluid is negligible compared to the temperature decrease of the hot fluid, as already described. The cause for this is the major difference in mass flow rates between the two streams. The effect can be seen in Figure 4.6, where the in- and outlet temperatures of the two streams are depicted as a function of the STHX length.

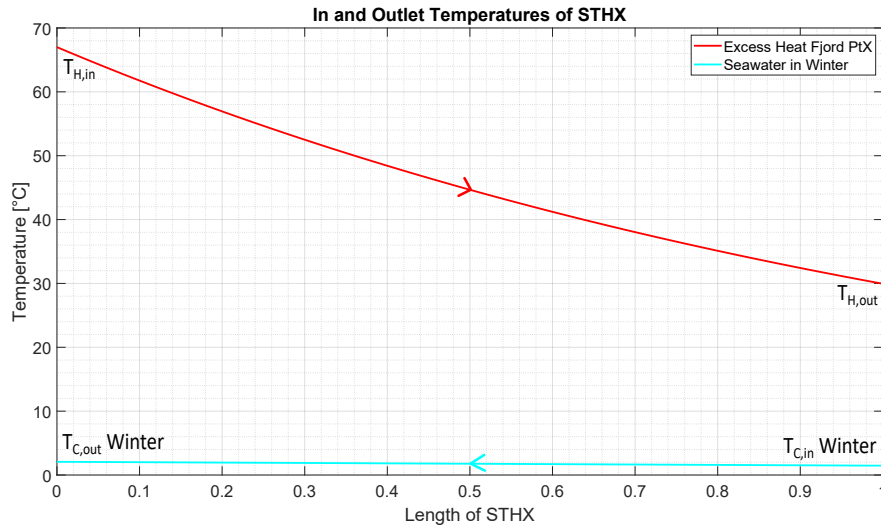


Figure 4.6: Temperature distribution curves in a counterflow STHX as the capacity ratio approaches zero because $\dot{C}_c \gg \dot{C}_h$.

It is clear that the temperature of the cold stream does not change significantly. The hot stream from Fjord PtX is cooled down from 67°C to 30°C and heat exchanges with the cold stream from the Limfjord Strait, which only gets a temperature increase of 0.6 K. This phenomenon is described by [Sanford and Gregory, 2009] where the conclusion is that the configuration of the heat exchanger configuration and the direction of the flows does not matter and the expression for NTU can be reduced and simplified and the problem be-

comes identical to an internal flow problem with a prescribed external temperature.

The pressure losses encountered in the STHX due to friction and minor losses are shown in Figure 4.7.

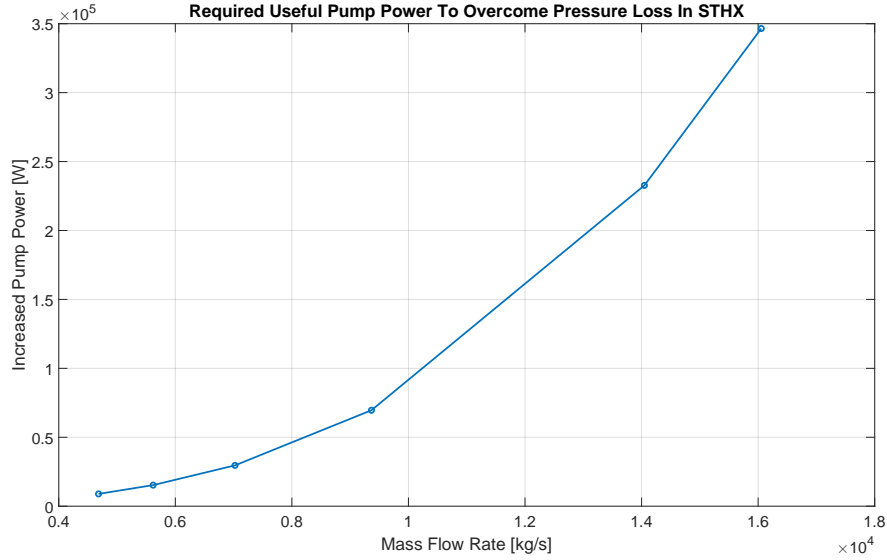


Figure 4.7: Increased pump power to overcome pressure losses in the STHX.

As expected, the required useful pump power increases with the mass flow rate, with a similar tendency. The small temperature rise and the added pump power indicate that further considerations and calculations are needed to determine if the introduction of the STHX is beneficial for the company.

4.3 Dynamic Transcritical Heat Pump Model with Hot Water Storage

In this Section, the dynamics of the *Hot Water Storage* (HWS) is investigated in order to predict and understand the tendencies within. The system will only be modelled with a hot water storage and will not include a *Cold Water Storage* (CWS) since the cold reservoir is essentially infinite. The HWS has a height of 33.61 meters and an inner radius of 21.76 meters, which results in a total volume of 50.000 m^3 . This is similar to one of the 4 new tanks that are being built at Aalborg Forsyning. The average heat transfer transmission coefficient is presumed constant at a value of $4 \frac{\text{W}}{\text{m}^2 \cdot \text{K}}$.

The HWS will be placed after the heat pump as shown in Figure 3.1 with the discretisation shown in Figure ???. The period in reference is a 48-hour period in LP1 from February 8th

to the 10th. The heating demand from 3.7b has been divided by 4, so it fits the model, which is just for one heat pump. The heat pump is set to run at full load for the whole period, as this LP1 period is a period with high demand for district heating. The inputs for the dynamic TC-HP model with HWS are seen based on the one without HWS, but the changes or additions are seen below:

- Constant mass flow of seawater into the evaporator: 4000 kg/s
- Constant mass flow of district heating water into the gas cooler: 210 kg/s
- Constant temperature from Limfjord Strait: 3°C
- Initial refrigerant temperature in refrigerant cycle: 0°C
- Return temperature of district heating water: 38°C
- Initial temperature of HWS top and bottom layer: 40 and 90°C with thermal stratification in place

The fluctuations in district heating demand shown in Figure 3.7b will influence the energy content of the HWS as well as the temperature distribution. The energy content is calculated with Equation (3.30) where the average temperature is the temperature of the middle layer. This is a fair assumption when the HWS is modelled as a uniformly stratified tank. The temperature is uniform in the horizontal plane. The energy content of the HWS in LP1 is seen in Figure 4.8.

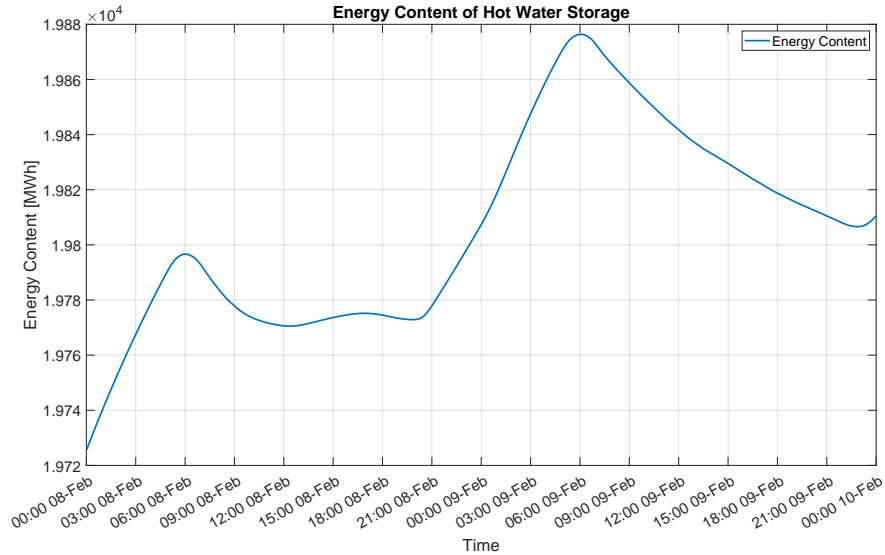


Figure 4.8: The energy content of the How Water Storage tank as a function of time, in the LP1 period of 48 hours.

It can be observed that the energy content of the HWS follows the trend of the DH demand. When there is low demand, the HWS is charged, and when the demand exceeds the capacity of the heat pumps 44.25 MW the energy content drops. It can also be seen that the rate at which the HWS is either charged or discharged is small, and the energy content only changes by around 160 MWh from the lowest to the highest energy mass.

This indicates that if the HWS initially has a high energy content, it is more than capable of supporting the DHN in those periods where the demand exceeds the heat pump's capacity. This will be hugely beneficial for the system and as a business case for Aalborg Forsyning since they can choose not to run the heat pump at times where the electricity prices are high and tap from the HWS. When the electricity prices, on the other hand, are low, they can run the heat pump and either cover the demand that way or also charge the HWS. Suppose the HWS is thermally insulated well, so the heat transfer to the surroundings is minimal. In that case, the HWS can easily be charged during hours or days with low electricity prices or when the DH demand is low or non-existent. After which it can be discharged when the electricity prices or the DH demand rise again.

The charging and discharging of the HWS in LP1 affect the thermal stratification in the HWS. The temperature of five selected layers is seen in Figure 4.9.

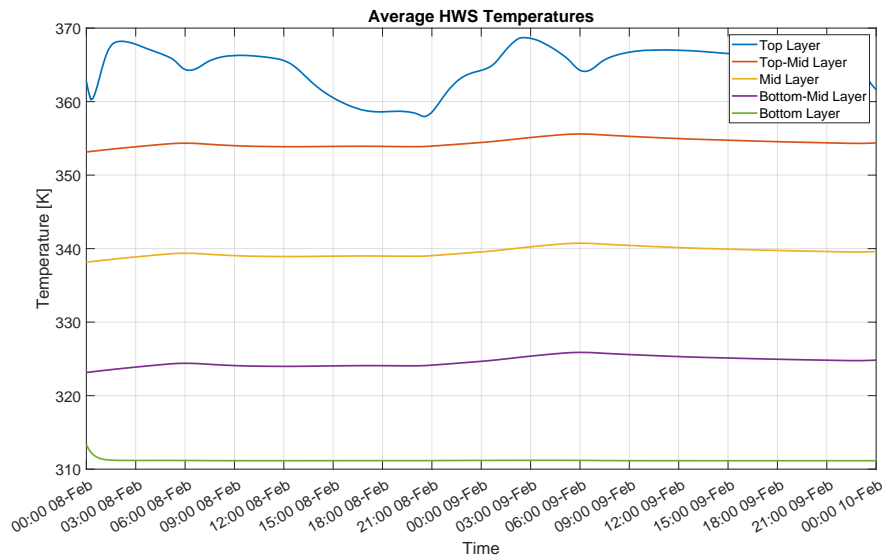


Figure 4.9: Temperature of five selected layers in the HWS as a function of the 48-hour period of LP1.

It is seen that the 4 lowest layers presented do not change significantly in temperature. However, the top layer does. This is due to the charging from the HP that enters this layer, and also the discharging to the DHN executed from this layer. This naturally creates a disturbance of the stratification that is mitigated downwards throughout the HWS. Notably the temperature of the top layer never exceeds the boiling point of water which is ideal.

The temperature is sometimes higher than 363.15 K (90°C), which is higher than what is needed in the DHN. This opens up for the possibility that water from the top layers can be shunted with colder water from another place for example excess heat, electric boiler or the HP when run in off-design.

The COP of the TC-HP with HWS is 2.4620, which is higher than the dynamic model of the TC-HP without HWS. This suggests that the HWS enables the TC-HP to work more efficiently. The P-h Diagram of the TC-HP with HWS is seen in Figure 4.10.

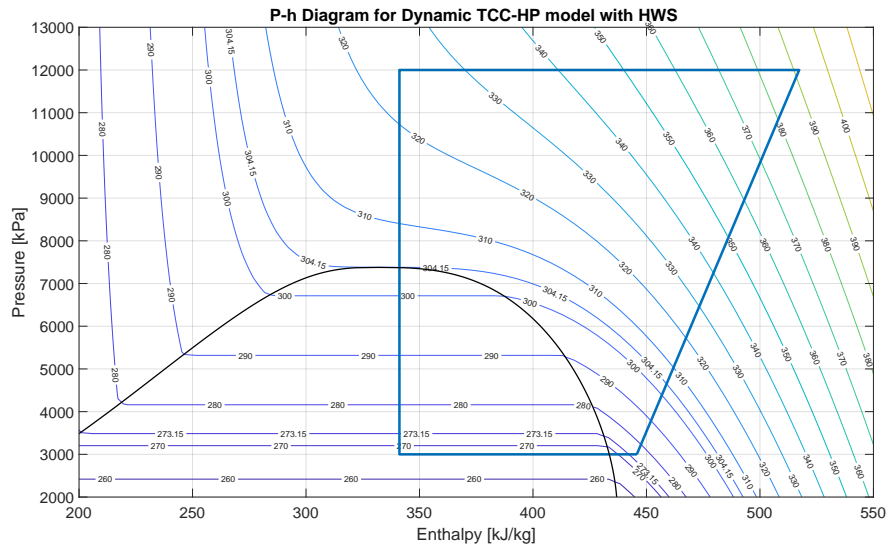


Figure 4.10: P-h Diagram of the TC-HP with HWS included

The results from this section is based from a period in February ie. LP1. Next a period in March will be investigated which corresponds to LP2.

4.3.1 Results from Transcritical Heat Pump Model with Hot Water Storage with Load Point 2 as Reference

The next period investigated is a 48-hour period from the 24th March to the 26th March, which will from here onwards be referred to as LP2. The DH demand for this period is seen in Figure 4.11.

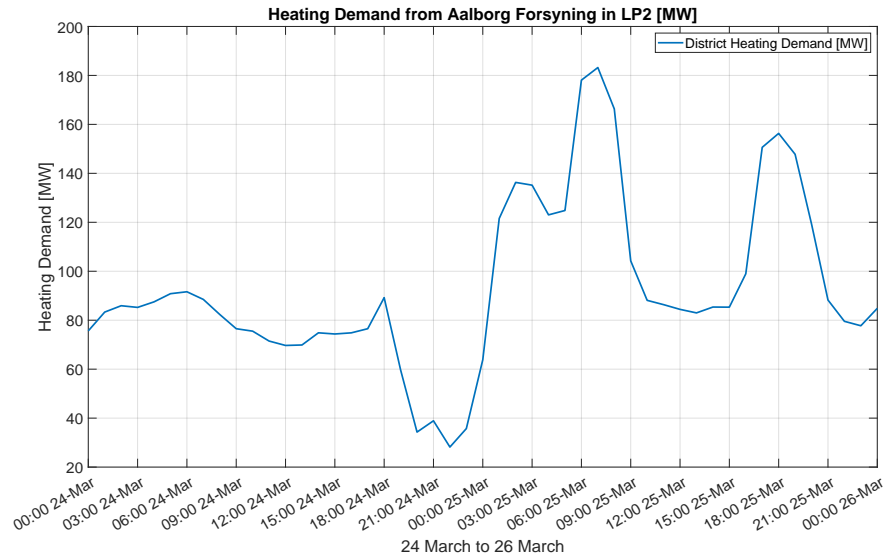


Figure 4.11: District heating demand in LP2

The district heating demand for LP2 is significantly lower, especially in the first 24 hours. This means that the HWS is going to be charged more than it is being discharged.

The energy content in the HWS throughout the 48-hour period is seen in Figure 4.12.

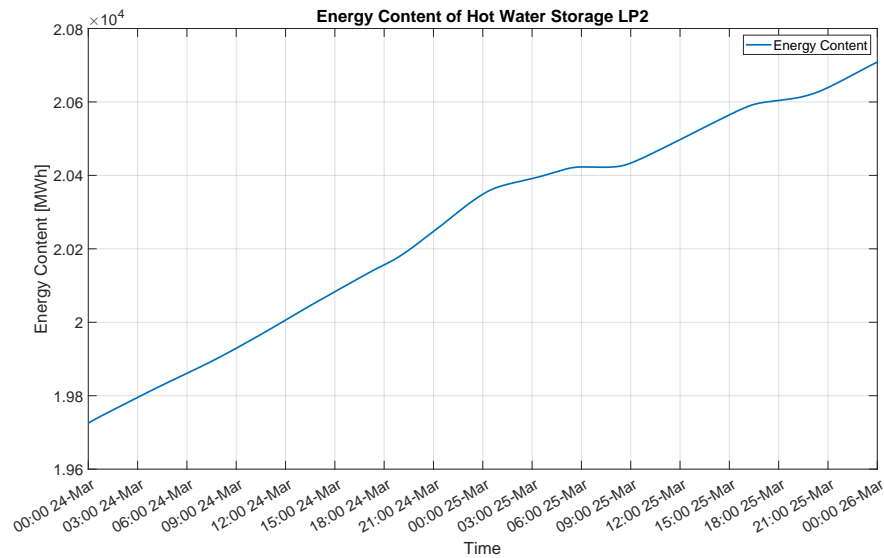


Figure 4.12: The energy content in the HWS in LP2

It is evident that the energy content of the HWS in LP2 rises steadily throughout the period. This is because the demand is constantly lower than the heat pump's capacity. The two peaks in the demand around 6 a.m. and 18 p.m. on March 25th bring the energy

content charging to a halt momentarily. The rate at which the HWS is charged is faster than LP1 and the energy content changes from 19,725 MWh to 20,708 MWh, so an increase of 983 MWh, which is over 6 times as much as the charging from LP1.

The investigation of LP3 and LP4 will not be made in this thesis, as this would likely reveal an even more exaggerated trend similar to LP2 with even lower district heating demand, higher surrounding temperatures, lower DH supply temperature from LP4 and higher DH return temperature for both LP3 and LP4.

4.4 Effects of Temperature Rise to the Evaporator by Heat Exchanging with Excess Heat

The final investigation is related to the excess heat from Fjord PtX and this thesis's main area of investigation. If the water inlet temperature to the evaporator is increased with excess heat, as seen in Figure 4.5, what will the increase in COP of the heat pump be?

The simulation is made without the HWS to simplify and focus on the TC-HP's performance. Similarly to the previous Section, simulations in LP1 and LP2 will be performed.

Initially, a scenario where the inlet water temperature to the evaporator is varied, and the other parameters are held constant, is performed. The mass flow of seawater into the evaporator is fixed at 4000 kg/s, which is a high mass flow for one heat pump of 44.25 MW. The variation of COP as a function of the seawater inlet temperature is seen in Figure 4.13.

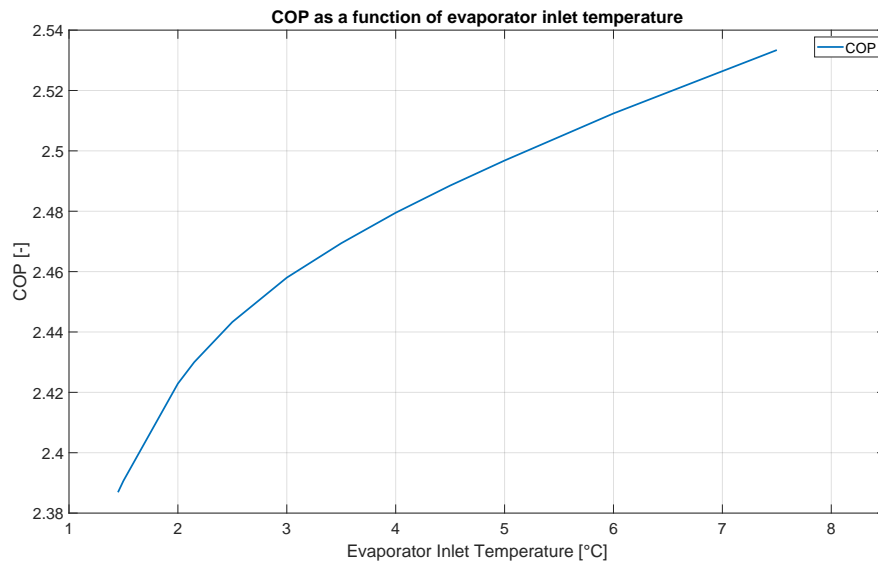


Figure 4.13: COP of the transcritical heat pump as a function of varying the inlet temperature to the evaporator.

It is shown that the COP of the heat pump does not change significantly with the variation of the evaporator inlet temperature. The increase is steeper at lower temperatures and becomes flatter at higher temperatures, and becomes close to linear. The higher the temperature in the evaporator, the higher the heat transfer increases, and the CO_2 can be superheated more before it enters the compressor. The temperature out of the evaporator also increases, and thus the overall COP increases.

Another cause for the slight increase in COP lies within the model itself. The compressor work is fixed, and as the evaporator temperature increases, the mass flow rate of CO_2 decreases, see Figure 4.14.

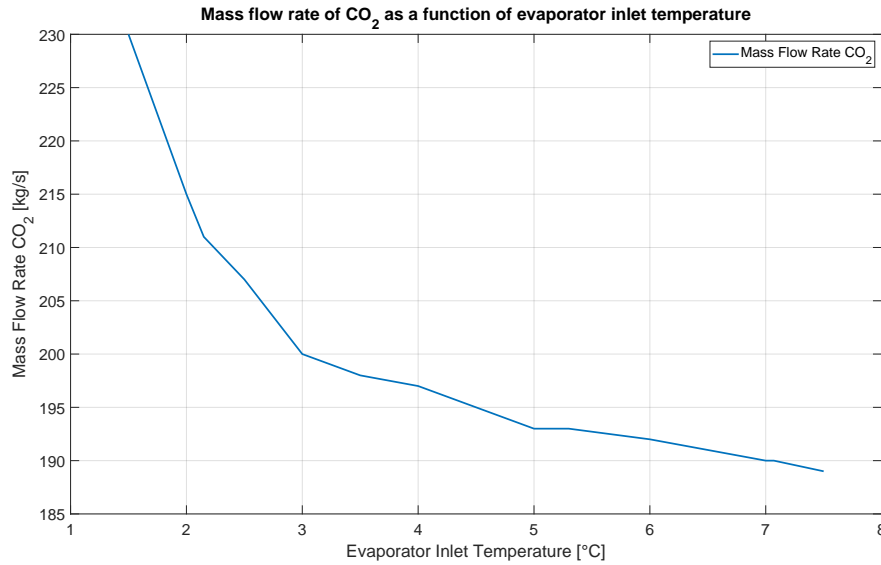


Figure 4.14: Mass flow rate of CO₂ variation as a function of the evaporator inlet temperature. As the evaporator inlet temperature increases, the mass flow rate of CO₂ decreases as the distance between isentropes becomes larger.

This is because the specific enthalpies before and after the compression increase each time the evaporator temperature increases, and the distance between the isentropes becomes wider.

The average temperature of the Limfjord Strait in the LP1 period from February 8th to February 10th is 1.45°C. With this low source temperature, the STHX will have to operate on a high mass flow rate, 14,000 kg/s for the 177 MW system or 3500 kg/s for just one 44.25 MW heat pump. This will result in a temperature lift of only 0.7 K in the STHX. The COP for the heat pump with an inlet temperature of 1.45°C is 2.3869 and increases to 2.43 after the rise of 0.7 K. This is an increase of 0.0431 in COP, which is seen as an insignificant gain in performance.

The average temperature of the Limfjord Strait in the LP2 period from the 24th of March to the 26th of March is 5.3°C. With this source temperature, the STHX is able to run at a lower mass flow rate of 5620 kg/s for the 177 MW system, and 1404 kg/s for just one 44.25 MW heat pump. This will result in a temperature lift of 1.77 K in the STHX. The COP for the heat pump with an inlet temperature of 5.3°C is 2.5015 and increases to 2.5271 after the temperature rise of 1.77 K. This is an increase of 0.0256 in COP, which is less of an improvement than LP1. The COP increase for LP1 and LP2 is presented in Figure 4.15.

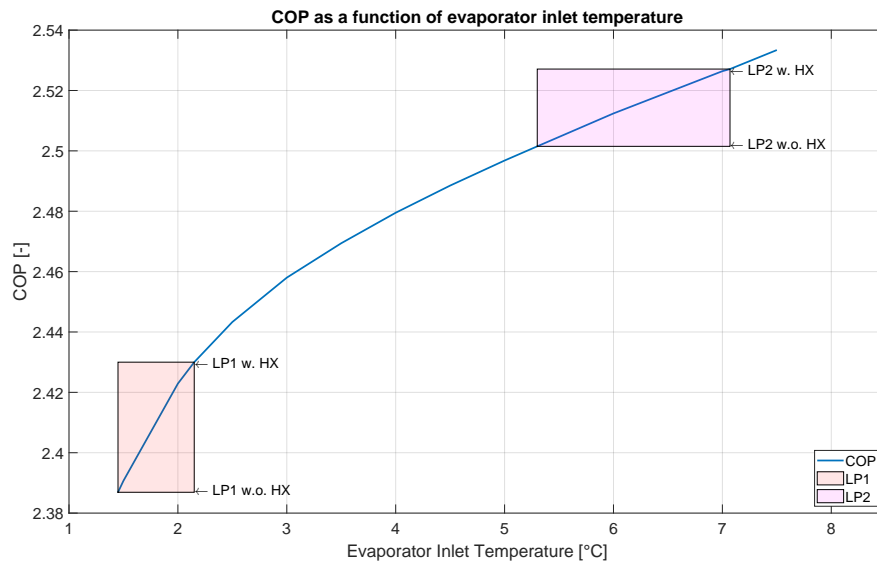


Figure 4.15: COP as a function of the evaporator inlet temperature. The shaded areas are the COP gain from LP1 and LP2 when evaluated with and without heat exchanging with the excess heat from Fjord PtX.

In the Figure, it is visually presented that the COP improvement from the heat exchange is not significant, although there is still a slight improvement. The reasons for this small improvement in COP lie within the basics of the heat pump's model and the thermodynamics surrounding it.

The increase in COP means that the heat pump can generate more heat per unit of electricity used in the compressor. If the 177 MW system is considered, the rise in COP for LP1 from 2.3869 to 2.43 means a reduction of 1315 kW per hour. For the 48-hour period, that adds up to 63,132 kWh. For LP2, it adds up to a reduction of 34,405 kWh in compressor work for the 48-hour period. These savings in electricity consumption will be considered further in the next chapter.

4.5 Improvements and Comments on the Heat Pump Configuration and System at Aalborg Forsyning

The heat pump at Aalborg Forsyning is, as mentioned, made up of four 44.25 MW heat pumps. These are not set up in any configuration where they are connected in either cascade or series connections. It is a huge benefit to have four heat pumps available, as there is more flexibility and freedom to manage the system. This section aims to give a short insight to some of the modification that could be made to the system, but not go into detail or any modelling since this thesis investigates the current system at Aalborg Forsyning.

4.5.1 Heat Pumps in Series

Heat pumps in series consist of two or more heat pumps connected in series. A benefit of heat pumps in series is that the temperature lift can be split up into smaller increments and thereby be done more controlled and efficiently. This is especially beneficial if the temperature lift is large or if there is a large temperature difference between the cold and hot reservoirs. The first heat pump in the series connection only needs to do part of the temperature lift, and the next heat pump will use the outlet temperature of the high temperature reservoir from the first heat pump as the inlet temperature for its high temperature reservoir. The same accounts for the low temperature reservoir. [Nielsen and Sørensen, 2020] investigated a case with five similar heat pumps connected in series with different temperatures in the evaporators and condensers (as it was sub-critical heat pumps), and the gain in COP was close to 1 compared to a single heat pump. This could also be a huge benefit in terms of flexibility when the seawater temperature and the DH demand change. The heat pumps can easily be decoupled or coupled when the DH demand changes. Lastly, different refrigerant combinations can be used in a heat pump in a series configuration. One refrigerant's main operation area could suit a heat pump working in the sub-critical area and then CO₂ as refrigerant for the supercritical area. A sketch of two heat pumps connected in series is seen in Figure 4.16.

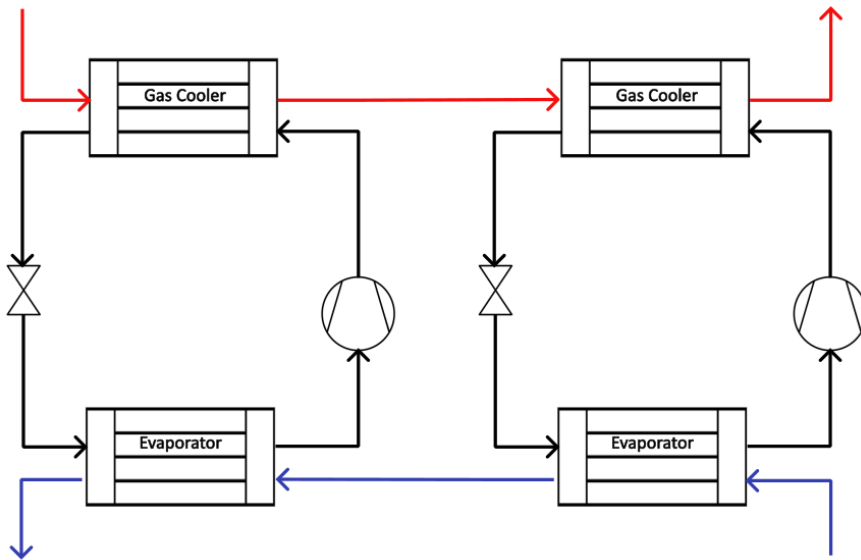


Figure 4.16: Two heat pumps in series connection

4.5.2 Heat Pumps in Cascade

In a heat pump in cascade configuration, the heat pump is split into a high-temperature heat pump and a low-temperature heat pump. The two cycles are connected via a 'cascade

heat exchanger' that works as the gas cooler/condenser for the low-temperature side and the evaporator for the high-temperature side. In Aalborg Forsynings' case, there could therefore be two of these cascade heat pumps instead of the four independent ones. A sketch of a cascade heat pump configuration is seen in Figure 4.17.

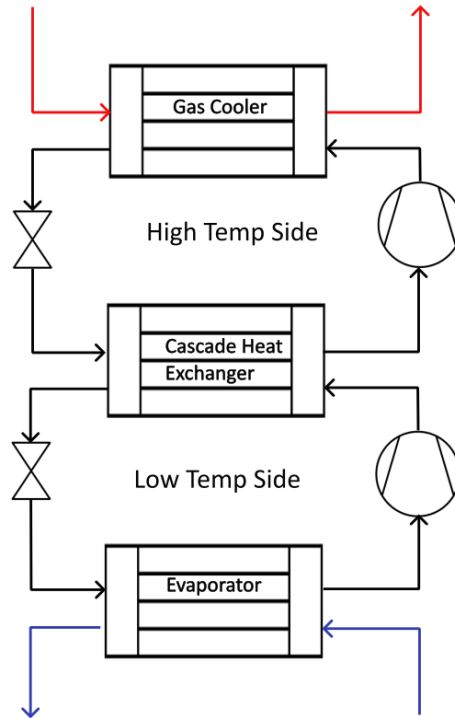


Figure 4.17: Two heat pumps connected in a cascade configuration. A high temperature side and low temperature side is present connected with a cascade heat exchanger.

A cascade system can also be beneficial when the temperature lift is large as once again the lift can be split up and be done more efficiently. It also allows for multiple refrigerants being used such as ammonia or butane for the low-temperature side and CO_2 for the high-temperature side.

4.5.3 Multistage Gas Cooling

[Yang et al., 2025] investigated a new type of three-stage gas cooling where the gas cooling is split into three separate heat exchangers. The three zones match the aforementioned temperature glide in the gas cooler, so one zone for the far sides of the minimum temperature approach and one zone in the middle close to the minimum temperature approach. This allows for much more precise control of the heat transfer.

4.5.4 Internal Heat Exchanger

An internal heat exchanger, or so-called recuperator, can be placed after the gas cooler and exchange heat with the exit of the evaporator. This ensures that there is no liquid in the mixture before it is compressed and therefore acts as the superheating of the vapour. In a TC heat pump cycle, this could work well with a two-stage expansion also, where there is an expansion valve for the first expansion down to the saturation line and one that expands it down to the evaporation pressure. A sketch of a heat pump with an internal heat exchanger/recuperator is seen in Figure 4.18.

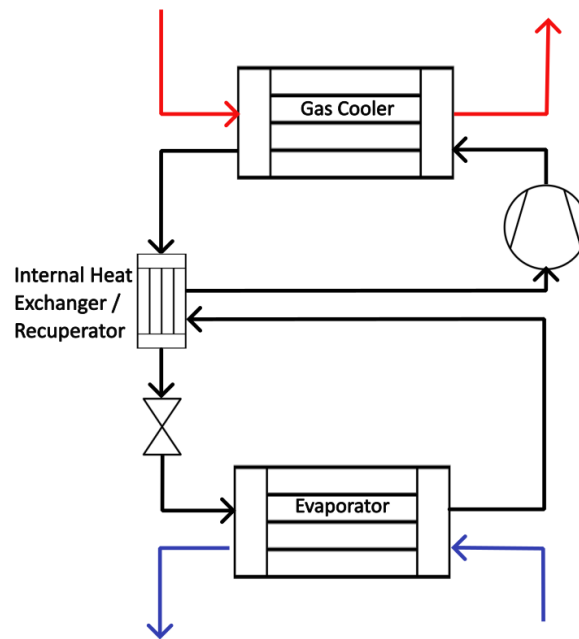


Figure 4.18: Heat pump cycle with an internal heat exchanger. This ensures only vapour enters the compressor.

Chapter 5

Techno-Economic Feasibility Analysis of Heat Exchanger Scenario

This Chapter presents the economic analysis of the STHX to determine whether it is a good business case for Aalborg Forsyning to implement such a device in their DHN. The heat pump's COP will be of great interest as this determines the electrical power needed for the system. The COP increase for the case with excess heat from Fjord PtX versus the case without excess heat will be considered. The capital expenses of the STHX and operational expenses for 20 years will be considered.

5.1 Cost Analysis

The base costs that are included in Chart 2.1 by [Smith, 2005] are from the year 2000 and it is, therefore, necessary to use the *Chemical Engineering Plant Cost Index* (CEPCI) to make the prices follow the inflation to present costs. The CEPCI from 2023 will be used and the CEPCI-index can be calculated as follows in Equation (5.1).

$$CEPCI_{INDEX} = \frac{CEPCI_{2000}}{CEPCI_{2023}} \quad (5.1)$$

Where $CEPCI_{2000}$ is 394.1 and for $CEPCI_{2023}$ is 800. This results in an INDEX of 0.4926.

5.1.1 Capital Expenses

The *Capital Expenses* (CAPEX) will be analysed by formulas and base costs from *Process Economics Report* by [Smith, 2005].

Cost data are often presented as cost versus capacity as expressed by Equation (5.2).

$$C_E = C_B \cdot \left(\frac{Q_{cm}}{Q_B} \right)^M \quad (5.2)$$

Where C_E is equipment cost with capacity measure Q_{cm} ie. for a heat exchanger it is the heat exchanger area seen in Table 3.1, C_B is the known base cost for equipment with base size Q_B and M is a constant depending on the equipment type.

There will be estimated correction factors for material due to the likelihood that the STHX will need to be built in an anti-corrosive material, such as titanium, which the evaporator in the TC-HP is made of. The material correction factor will be multiplied by Equation (5.2), hereby Equation (5.3) is obtained.

$$C_E = C_B \cdot \left(\frac{Q_{cm}}{Q_B} \right)^M \cdot f_M \quad (5.3)$$

Where f_M is the material correction factor, which is 5.8 for titanium. For the present CAPEX, the CEPCI Index is divided by C_E , as seen in Equation (5.4).

$$C_{E,Present} = \frac{C_E}{CEPCI_{INDEX}} \quad (5.4)$$

The CAPEX of the STHX amounts to €2.45M. This is the total equipment cost without installation costs for piping, electrical equipment, etc. The total CAPEX of the installed battery limits equipment will normally be two to four times higher than the total equipment cost [Smith, 2005]. This could be up to 6 times the CAPEX for fluid processes with high stress.

The cost for retrofitting, which is the case in the STHX for Aalborg Forsyning, is more difficult than estimating the cost for an entirely new design/system [Smith, 2005]. Some equipment of the existing network could be reused, while some might need to be replaced. Furthermore, the costs of ‘downtime’ of the plant need to be considered. The costs of the lost production of heat can be added to the total cost of the retrofit. In the case of retrofitting an STHX to the Limfjord seawater channel, it could be planned during the summer, where the heat pump is scheduled to be shut down or to operate at a minimum, see LP3 and LP4 in Table 3.2.

For the total CAPEX of retrofitting the TC-HP system with the STHX, with installation costs included, a factor of 6 times the total equipment cost will be used. This results in the total CAPEX estimated to be €14.7M. This considerable investment raises questions about whether a plate-HX would be a cheaper alternative.

5.1.2 Operational Expenses

The *Operational Expenses* (OPEX) are determined as the energy requirement for the system, ie, the cost of electricity. With a higher COP, the heat pump is more efficient and consumes less electricity for the same heat output. The fluctuations in electricity prices can influence the OPEX significantly, and a system like the one at Aalborg Forsyning would be beneficial with a long-term contractual agreement with the transmission system operator. The electricity price used for the calculations of OPEX in this thesis is set at €75/MWh without tariffs, which has been taken from Nord Pools Market Data [Pool, 2025].

The operational expenses of the TC-HP are based on the COP. The COP used are the ones estimated by the dynamic model, even though they are underestimated. The main focus is to determine if the case with excess heat is a better business case than without it.

The OPEX is determined from the COP of the heat pump in the four LPs, after which they are multiplied by the amount of time that the heat pump operates in that period. Given from Table 3.2, LP1 accounts for 40%, LP2 for 30%, LP3 for 20% and LP4 for 10% of the total operation time of 4000 hours a year.

5.1.3 Present Worth Value

The economic analysis will conclude with a *Present Worth Value* (PWV). The PWV of an amount of money represents the today's value of a sum of money to be received in the future. The PWV is calculated in Equation (5.5).

$$PWV = V_n \cdot \left(\frac{1}{(1 + r_i)^n} \right) \quad (5.5)$$

Where PWV is the present worth value, V_n is the value to be received or paid per n periods in the future (revenue minus OPEX) and r_i is the interest rate. In this project, n is equal to 20 years and r is equal to 4%..

The revenue in this analysis is taken from the annual DH demand managed by the heat pump and the price at which DH is sold. The price of DH is €0.13/KWh without VAT and the annual heating demand provided by the heat pump at Aalborg Forsyning is 700M kWh. This totals a revenue pick up of €74.2M/year.

5.1.4 Results of Present Worth Value

The results of the economic analysis, as well as other parameters, are presented in Table 5.1.

Table 5.1: Results of the economic data.

Variable	Value	
Interest Rate	4	[%]
Plant Life Time	20	[yr]
Revenue	74.2M	[€/yr]
CAPEX STHX	14.7M	[€]
OPEX LP1 w. HX	9.353M	[€/yr]
OPEX LP1 w.o HX	9.491M	[€/yr]
OPEX LP2 w. HX	6.730M	[€/yr]
OPEX LP2 w.o HX	6.792M	[€/yr]
OPEX LP3 w. HX	4.393M	[€/yr]
OPEX LP3 w.o HX	4.436M	[€/yr]
OPEX LP4 w HX	2.135M	[€/yr]
OPEX LP4 w.o HX	2.156M	[€/yr]
OPEX Total w HX	22.612M	[€/yr]
OPEX Total w.o HX	22.877M	[€/yr]
OPEX Net Difference	0.248M	[€/yr]
CEPCI 2000	394.1	[-]
CEPCI 2023	800	[-]
CEPCI INDEX	0.4926	[-]

It should be noted that the revenue is for the entire heat pump system, and the OPEX of the respective LPs are only for the TC-HP with or without the extra pump power from the STHX. Two cases will be made, where case 1 has a revenue pick-up and case 2 does not have a revenue pick-up. In case 2, without revenue pickup, the one with the least negative PVW after the 20-year period is the best solution.

The results of the PVW analysis for case 1 with revenue pick-up are seen in Figure 5.1.



Figure 5.1: Present Worth Value with revenue pick-up. The electricity price is € 75/MWh and the interest rate is 8%

As shown in the analysis, the PVW with the STHX implemented for excess heat implementation ends up with a lower value than the PVW without the STHX. The €0.248M lower OPEX for the STHX scenario is not enough to compensate for the high CAPEX. After 20 years, the STHX scenario's PVW is €11.3M lower than the one without excess heat. It is also seen that the PVW breaks even in the first year already. This is linked to the fact that only the CAPEX of the STHX is considered in this PVW analysis and not the TC-HP, which is confidential.

As mentioned earlier, the revenue considered in this analysis is taken from the entire DH demand and is a bit distorted and/or misleading. Therefore, a case without the revenue pick-up is also considered. This case is seen in Figure 5.2.



Figure 5.2: Present Worth Value without revenue pick-up. The electricity price is €75/MWh and the interest rate is 8%

Both systems have a negative PWV, as expected, but the PWV from the scenario without the HX and excess heat is the least negative.

This concludes the economic analysis, which shows that even though the excess heat increases the COP of the heat pump and thereby decreases the electricity consumption and lowers the OPEX, the CAPEX of the STHX is so substantial that the PWV for the scenario with the heat exchanging still becomes a non favorable business case.

Further considerations to the economic analysis would be to implement a tool to calculate the lost revenue when the heat pump is shut down due to seawater temperature being too low. In recent years, the winters in Denmark have been mild. In fact, only 500 hours over the last five years have been with temperatures below what is feasible to operate the heat pump. In those days the HWS should be able to handle the DH demand.

Chapter 6

Conclusion

The objective of this master's thesis was to investigate the behaviour of a 177 MW transcritical CO₂ heat pump at Aalborg Forsyning. The heat pump is a state-of-the-art seawater heat pump whose purpose is to support the district heating network and be a supplement to the old coal-fired combined heat and power plant, Nordjyllandsværket 3. The heat pump's heat source is the nearby Limfjord Strait, whose temperature changes throughout the year. A stream of excess heat from the nearby future Power-to-X facility will be heat exchanged with the inlet to heat pump and the effects have been investigated.

A steady-state model of one of the 44.25 MW heat pumps was implemented and the results showed a COP of 3.35. As CO₂ operates in the supercritical region where the thermo-physical properties can change quickly, the gas cooler and evaporator were discretised. This allowed for precise heat transfer measurements. The dynamic model includes this discretisation of the evaporator and the gas cooler. The periods of simulation were split into four Load Points (LPs), which mimicked the periods given by MAN Energy Solutions. LP1 and LP2 were of greatest interest as these are in periods of low seawater temperature. The dynamic model showed a COP of 2.33, which is significantly underestimated from the steady state model. Some tweaking to the model is suggested. The model showed a temperature glide in the gas cooler that matches the literature, where the minimum temperature approach is located near the middle of the gas cooler length. The dynamic model showed a quick startup time for the heat pump of approximately 5 minutes from 20% to 80% load.

The dynamic model included a *Hot Water Storage* (HWS) after the heat pump cycle to add to the flexibility. The HWS was modelled after a thermally stratified principle as a convective-diffusive problem. The discretisation of the HWS was a method of lines approach treated with different schemes depending on the resulting flow direction inside the HWS. Shaping functions and limiter functions were applied to account for spatial oscillations and sharp transitions.

The implementation of the HWS in the dynamic transcritical heat pump model showed the energy content increasing in the LP1 and LP2 periods with thermal stratification in the respective layers. In the top layer where loading and tapping are present, the stratification showed some disturbances. The HWS was deemed an excellent support for the system and allows for sector coupling when electricity prices fluctuate.

The heat exchanger has been modelled as a *Shell-and-Tube Heat Exchanger* (STHX) with one shell pass and two tube passes. The STHX was modelled after the ϵ -NTU method, which showed a moderate effectiveness between 0.56 and 0.78. The capacity ratio between the

two streams was close to zero due to the substantial difference between the mass flow rates.

The seawater inlet stream to the evaporator showed a temperature rise between 0.6 and 2.3 K, depending on the mass flow rate of the cold stream and assuming the maximum excess heat quantity from the PtX facility. The low temperature increase is present when the seawater temperature is lowest and the mass flow rate has to be the highest. This small temperature rise is not significant. The STHX dimensions also showed that a large HX area and long pipes are needed. This added to the increased pressure losses and economics.

The dynamic transcritical heat pump model investigated the COP as a function of the temperature rise of the inlet into the evaporator. The results showed a steep increase in COP at low temperatures and lower positive effects at higher temperatures. The COP increase for scenarios with and without the excess heat showed an increase in COP for LP1 of 0.0431 and 0.0256 for LP2, which is moderate.

The techno-economic feasibility analysis indicated that the STHX's CAPEX was estimated to be €14.7M. Furthermore, the COP gain for the four LPs was considered in terms of the lower electrical consumption by the heat pump. The COP increase results in a yearly reduction in OPEX of €0.248M. The conclusion is that the STHX is too expensive to construct and retrofit compared to the small performance gain of the HP and the hereby related lowered electricity consumption.

Chapter 7

Future Work

This master thesis investigates the transcritical CO₂ heat pump at Aalborg Forsyning, along with a heat exchanger analysis to increase the temperature into the evaporator inlet by a stream of excess heat. This Chapter aims to discuss and explore the possible future changes and improvements to the model.

7.1 Heat Exchanger Variations

The heat exchanger investigated in this thesis was a shell-and-tube heat exchanger. This was decided for two reasons. The effective-NTU method and cost analyses supported this technology. Investigating other heat exchanger configurations, such as the plate heat exchanger, would be beneficial. This would require some literature study or knowledge sharing with manufacturers. The plate heat exchanger has attributes that make it a solid candidate for an alternative to the STHX modelled in this thesis.

7.2 Parameter Study for Dynamic Heat Pump Model

A parameter study of the dynamic heat pump model, where different parameters should be varied, would strengthen the understanding of the model. Like the start-up time was investigated and determined to be approximately 5 minutes from 20 to 80%, a shutdown period could be investigated to determine the flexibility of the heat pump to further add to the sector-coupling.

Other parameters to be varied could include the pressure in the gas cooler and evaporator. This could also lead to a better understanding of why the dynamic heat pump model tends to underestimate the COP.

7.3 Different Heat Pump Configurations and Adjustments

As mentioned in Section 4.5, different configurations or adjustments to the heat pump could be investigated. Either with the four heat pumps in series, four by one or two by two. Cascade configuration with different refrigerants in the low-temperature side and high-temperature side. Lastly, the implementation of an internal heat exchanger for better representation of the proposed configuration from MAN could be implemented. This would allow for more precise control of the superheating of the vapour before the compression.

7.4 Statistical Analysis of Seawater Temperatures

The average temperature used in this model is taken as an average from the past 15 years. It would be more accurate to also use some deviations and outliers, and link this with the standard deviation. Then the 10, 25, 75 and 90 percentiles for each LP could be used for a stronger statistical analysis. Furthermore, a tool to determine what would happen on days when the temperature is too low for the heat pump to function.

Bibliography

- [Aalborg Forsyning, 2024] Aalborg Forsyning (2024). Fjernvarmedeklaration 2023. <https://aalborgforsyning.dk/privat/fjernvarmedeklaration-2024/>. Last accessed 12th of February 2025.
- [Aalborg Forsyning, 2025] Aalborg Forsyning (2025). Talks and meetings with aalborg forsyning. Last accessed 14th of March 2025.
- [Aalborg Portland, 2025] Aalborg Portland (2025). Aalborg portland underskriver aftale med eus innovationsfond om milliardstøtte til co2-fangst. Last accessed 14th of March 2025.
- [Danfoss, 2023] Danfoss (2023). Co2 as refrigerant in cooling and heating systems fundamentals & applications. <https://assets.danfoss.com/documents/latest/356557/BE470937803806en-000101.pdf>. Last accessed 25th of February 2025.
- [Dansk Fjernvarme, 2023] Dansk Fjernvarme (2023). Fjernvarmens rolle i energisystemet. <https://danskfjernvarme.dk/viden-vaerktoejer/udgivelser/fjernvarmens-rolle-i-energisystemet>. Last accessed 11th of February 2025.
- [Dansk Fjernvarme, 2024] Dansk Fjernvarme (2024). Standardhuset er forældet: Så lidt varme bruger en gennemsnitlig husholdning med fjernvarme. Last accessed 14th of March 2025.
- [Fjord PTX, 2025] Fjord PTX (2025). Fjord ptx aalborg. <https://www.fjord-ptx.dk/>. Last accessed 14th of March 2025.
- [Holten et al., 2012] Holten, A., Solsona, H., Eider, P. U. R., and Houbak-Jensen, L. (2012). Dynamic model of co2 heat pump and thermal storages- implemented in a conceptual chp plant with flue gas heat recovery. https://kdbk-aub.primo.exlibrisgroup.com/permalink/45KBDK_AUB/a7me0f/alma9921562511305762. Last accessed 19th of March 2025.
- [KEFM, 2025] KEFM (2025). Aftale om afskaffelse af prisloft på overskudsvarme. <https://www.kefm.dk/Media/638726962329939023/Aftale%20om%20afskaffelse%20af%20prisloft%20p%C3%A5%20overskudsvarme.pdf>. Last accessed 11th of February 2025.
- [Kreuzinger et al., 2008] Kreuzinger, T., Bitzer, M., and and, W. M. (2008). Mathematical modelling of a domestic heating system with stratified storage tank. *Mathematical and Computer Modelling of Dynamical Systems*, 14(3):231–248.
- [MAN, 2023] MAN (2023). Man heat pumps for district heating. <https://global.gotowebinar.com/api/handouts/720d905f55bf49b881ec788f9856063d/file?X-Amz-Algorithm=AWS4-HMAC-SHA256&X-Amz-Date=20250210T152919Z&X-Amz-SignedHeaders=>

- host&X-Amz-Expires=86399&X-Amz-Credential=AKIAZVFEQAKQEY26RD45%
2F20250210%2Fus-east-1%2Fs3%2Faws4_request&X-Amz-Signature=
a23fec5cd3b2af736d3c1c9457a6d14401e43c9f8aecde04154dbd6a6b9e19f8. Last
accessed 11th of February 2024.
- [MAN, 2025] MAN (2025). Man energy solutions to deliver additional heat pump unit for
aalborgs district heating. Last accessed 17th of February 2025.
- [Mathworks, 2025] Mathworks (2025). ode15s. [https://se.mathworks.com/help/
matlab/ref/ode15s.html](https://se.mathworks.com/help/matlab/ref/ode15s.html). Last accessed 19th of March 2025.
- [Nielsen and Sørensen, 2020] Nielsen, M. P. and Sørensen, K. (2020). Dynamic modeling
of heat pumps for ancillary services in local district heating concepts. Last accessed 19th
of March 2025.
- [Pool, 2025] Pool, N. (2025). Day-ahead prices. [https://data.nordpoolgroup.
com/auction/day-ahead/prices?deliveryDate=2024-05-24¤cy=EUR&
aggregation=MonthlyAggregate&deliveryAreas=DK1](https://data.nordpoolgroup.com/auction/day-ahead/prices?deliveryDate=2024-05-24¤cy=EUR&aggregation=MonthlyAggregate&deliveryAreas=DK1). Last accessed 23th of May
2025.
- [Sanford and Gregory, 2009] Sanford, K. and Gregory, N. (2009). *Heat Transfer*. Cambridge
University Press. ISBN: 978-0-521-88107-4.
- [Smith, 2005] Smith, R. (2005). Chemical process design and analysis. ISBN: 0-471-48680-9.
- [Span and Wagner, 2002] Span, R. and Wagner, W. (2002). Equations of state
for technical applications. [https://www.studocu.com/en-gb/document/
the-university-of-edinburgh/chemical-engineering-thermodynamics-3/
span-wagner-2003-article-equations-of-state-for-technical-ap/14298678](https://www.studocu.com/en-gb/document/the-university-of-edinburgh/chemical-engineering-thermodynamics-3/span-wagner-2003-article-equations-of-state-for-technical-ap/14298678).
Last accessed 12th of May 2025.
- [United Nations Climate Change, 2022] United Nations Climate
Change (2022). The paris agreement. [https://unfccc.int/
process-and-meetings/the-paris-agreement/the-paris-agreement?
gclid=CjwKCAiA3KefBhByEiwAi2LDHFXPgxxSAJSzqJPCsUEqhx9w2H0FY_BT_
JzVLpa6LONWbJb6LXY1JhoCVWYQAvD_BwE](https://unfccc.int/process-and-meetings/the-paris-agreement/the-paris-agreement?gclid=CjwKCAiA3KefBhByEiwAi2LDHFXPgxxSAJSzqJPCsUEqhx9w2H0FY_BT_JzVLpa6LONWbJb6LXY1JhoCVWYQAvD_BwE). Last accessed 13th of February 2022.
- [VDI, 2010] VDI (2010). Vdi heat atlas. [https://link.springer.com/referencework/10.
1007/978-3-540-77877-6](https://link.springer.com/referencework/10.1007/978-3-540-77877-6). Last accessed 19th of March 2025.
- [Yang et al., 2025] Yang, L., Wang, X., Xu, B., and Chen, Z. (2025). Experimental study on
the efficient heating of transcritical co2 heat pumps based on heat capacity and thermal
quality analysis. *Applied Thermal Engineering*, 270:126219.
- [Yunus A. et al., 2016] Yunus A., C., John M., S., and Robert H., T. (2016). *Fundamentals of
Thermal-Fluid Sciences*. McGraw-Hill Education - Europa. ISBN: 9789814720953.

[Zhang and Yamaguchi, 2021] Zhang, X.-R. and Yamaguchi, H. (2021). *Transcritical CO₂ Heat Pump Fundamentals and Applications*. Wiley. ISBN: 9781118380048.

Appendix A

A.1 Additional Equations for Hot Water Storage

Boundary conditions for the PDEs in the HWS. These are described by [Kreuzinger et al., 2008].

$$L = 0, v > 0 : \quad Mc_p \frac{\partial T}{\partial t} = kA \frac{\partial^2 T}{\partial z^2} dz + \dot{m}_{BL} c_p T_{BL} - \dot{m}_{BT} c_p T_B + \dot{m}_c c_p T_B - hA_s (T - T_a) \quad (\text{A.1})$$

$$L = 0, v < 0 : \quad Mc_p \frac{\partial T}{\partial t} = kA \frac{\partial^2 T}{\partial z^2} dz + \dot{m}_{BL} c_p T_{BL} - \dot{m}_{BT} c_p T_B + \dot{m}_c c_p T_B - hA_s (T - T_a) \quad (\text{A.2})$$

$$L = h, v > 0 : \quad Mc_p \frac{\partial T}{\partial t} = kA \frac{\partial^2 T}{\partial z^2} dz + \dot{m}_{TL} c_p T_{TL} - \dot{m}_{TT} c_p T_T + \dot{m}_c c_p T_T - hA_s (T - T_a) \quad (\text{A.3})$$

$$L = h, v < 0 : \quad Mc_p \frac{\partial T}{\partial t} = kA \frac{\partial^2 T}{\partial z^2} dz + \dot{m}_{TL} c_p T_{TL} - \dot{m}_{TT} c_p T_T + \dot{m}_c c_p T_T - hA_s (T - T_a) \quad (\text{A.4})$$

Where the notations are TT - Top Tap, TL - Top Load, BL - Bottom Load and BT - Bottom Tap.